Engineering Autonomous Chemomechanical Nanomachines Using Brownian Ratchets

Gabriel Lavella

Electrical Engineering and Computer Sciences
University of California at Berkeley

Technical Report No. UCB/EECS-2012-221
http://www.eecs.berkeley.edu/Pubs/TechRpts/2012/EECS-2012-221.html

December 1, 2012

Engineering Autonomous Chemomechanical Nanomachines Using Brownian Ratchets

by

Gabriel Lavella

A dissertation submitted in partial completion of the

requirements for the degree of

Doctor of Philosophy

in

Electrical Engineering

in the

Graduate Division of the

University of California, Berkeley

Committee in charge:

Professor Michel M. Maharbiz, Chair
Professor Kristofer S.J. Pister
Professor Dorian Leipmann

Fall 2011

Engineering Autonomous Chemomechanical Nanomachines Using Brownian Ratchets

By Gabriel Lavella

Abstract

Engineering Autonomous Chemomechanical Nanomachines Using Brownian Ratchets

by

Gabriel Lavella

Doctor of Philosophy in Electrical Engineering

University of California, Berkeley

Professor Michel M. Maharbiz, Chair

Nanoscale machines which directly convert chemical energy into mechanical work are ubiquitous in nature and are employed to perform a diverse set of tasks such as transporting molecules, maintaining molecular gradients, and providing motion to organisms. Their widespread use in nature suggests that large technological rewards can be obtained by designing synthetic machines that use similar mechanisms.

This thesis addresses the technological adaptation of a specific mechanism known as the Brownian ratchet for the design of synthetic autonomous nanomachines. My efforts were focused more specifically on synthetic chemomechanical ratchets which I deem will be broadly applicable in the life sciences. In my work I have theoretically explored the biophysical mechanisms and energy landscapes that give rise to the ratcheting phenomena and devised devices that operate off these principles.

I demonstrate two generations of devices that produce mechanical force/deformation in response to a user specified ligand. The first generation devices, fabricatied using a combination nanoscale lithographic processes and bioconjugation techniques, were used to provide evidence that the proposed ratcheting phenomena can be exploited in synthetic architectures. Second generation devices fabricated using self-assembled DNA/hapten motifs were constructed to gain a precise understanding of ratcheting dynamics and design constraints. In addition, the self-assembled devices enabled fabrication en masse, which I feel will alleviate future experimental hurdles in analysis and facilitate its adaptation to technologies.

The product of these efforts is an architecture that has the potential to enable numerous technologies in biosensing and drug delivery. For example, the coupling of molecule-specific actuation to the release of drugs or signaling molecules from nanocapsules or porous materials could be transformative. Such architectures could provide possible avenues to pressing issues in biology and medicine: drugs could eventually be triggered to release in the presence of molecular signals indicative of diseased states, early disease detection could be achieved by examining the cell microenvironment then releasing imaging agents and generalized control could exerted over the free molecule signaling networks of cells.

Contents

List of Figures

List of Tables

Chapter 1

Natural Brownian Ratchet Systems and Classifications

1.1 Motivation

Perhaps the most alluring prospect for autonomous nanomachines is their capacity for molecular-level interaction with biological systems. The rationale for this is clear: sophisticated interaction may necessitate a device of sufficiently small scale to navigate through cell-scale topology and remain unobtrusive to cell function. Within organisms, cells communicate via chemical and mechanical exchanges mediated by molecular signaling networks. These networks control the sequence of events that give rise to the organism's morphology, behavior and function. In my work I sought to understand if devices could be built – without the need for novel enzyme design – that can detect and mediate these chemical signals. More specifically, was it possible to build a generic, soluble transducer that detects one signal moiety and mechanically react with great specificity and signal adaptability? Further could this mechanical response be coupled to a meaningful output or a means to exert control over the signaling network? Figure 1.1 provides a notional illustration of this concept.

One mechanism called the *Brownian ratchet* provides a possible means to enable this form of transduction. Evidence for this exists in numerous natural systems. With this in mind, I conceived a ratchet structure that would achieve user specified chemomechanical conversion. This structure, which is described in detail in Chapters 2, 3 and 4, can be fabricated by controlling the assembly of molecules over the order of tens of nanometers – a challenge far simpler than those presented by molecular engineering.

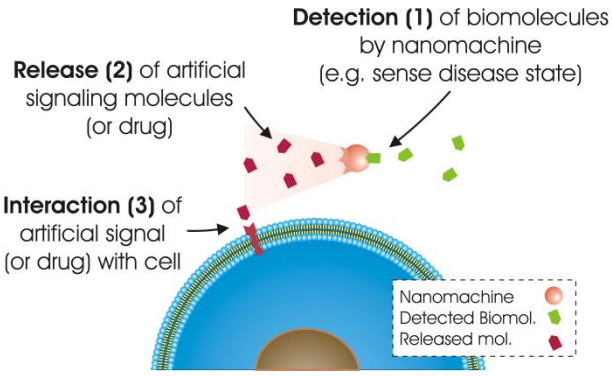

Figure 1.1 Conceptual overview of cellular artificial signal transduction using a nanomachine.

The use of Brownian ratchet architectures in the design of chemomechanical nanomachines remains a relatively unexplored space, yet numerous fabrication techniques have recently become available to facilitate in their construction. These include both top down assisted methods, such as template assisted pattering, various forms of DNA origami and phage display engineering.

In the long term I hope to adapt the Brownian ratcheting architecture toward creating a machine capable of detecting one signal and transducing that into to the release of a secondary species. In this case the secondary species would be interchangeable because it is tied to the mechanical response and not to a particular reaction. This implementation could lay the foundation for several meaningful technologies; drugs could be released directly in local microenvironment in response to free biomarkers, molecular markers for diseases could be detected in the cell

microenvironment and imaging agents could be released for early disease detection. A conceptualization of these possibilities is shown in Figure 1.2.

1.2 Natural Brownian Machines

Nanoscale machines which directly convert chemical energy into mechanical work are ubiquitous in nature and are employed to perform a diverse set of tasks such as transporting molecules, maintaining molecular gradients, and providing motion to organisms.[1] Numerous forms exist, categorized as biological motors, rotors, shuttles, springs and ratchets.[2] By and large, these devices are powered by energy extracted from concentration gradients, the breaking or formation of covalent bonds - most notably ATP, NADH, and NADPH - or in the case of ratchet type mechanisms from polymerization reactions.[3] The extensive study of their operation has provided scientists with empirical demonstrations of the mechanisms by which nanoscale machines can operate. They suggest that in a nanoscale environment where viscous and thermal forces dominate inertia, structures that perform chemomechanical transduction are well served by biasing random thermal movements with asymmetries in the energy landscape. This design strategy, allows devices to accomplish directed motion against thermal fluctuations.

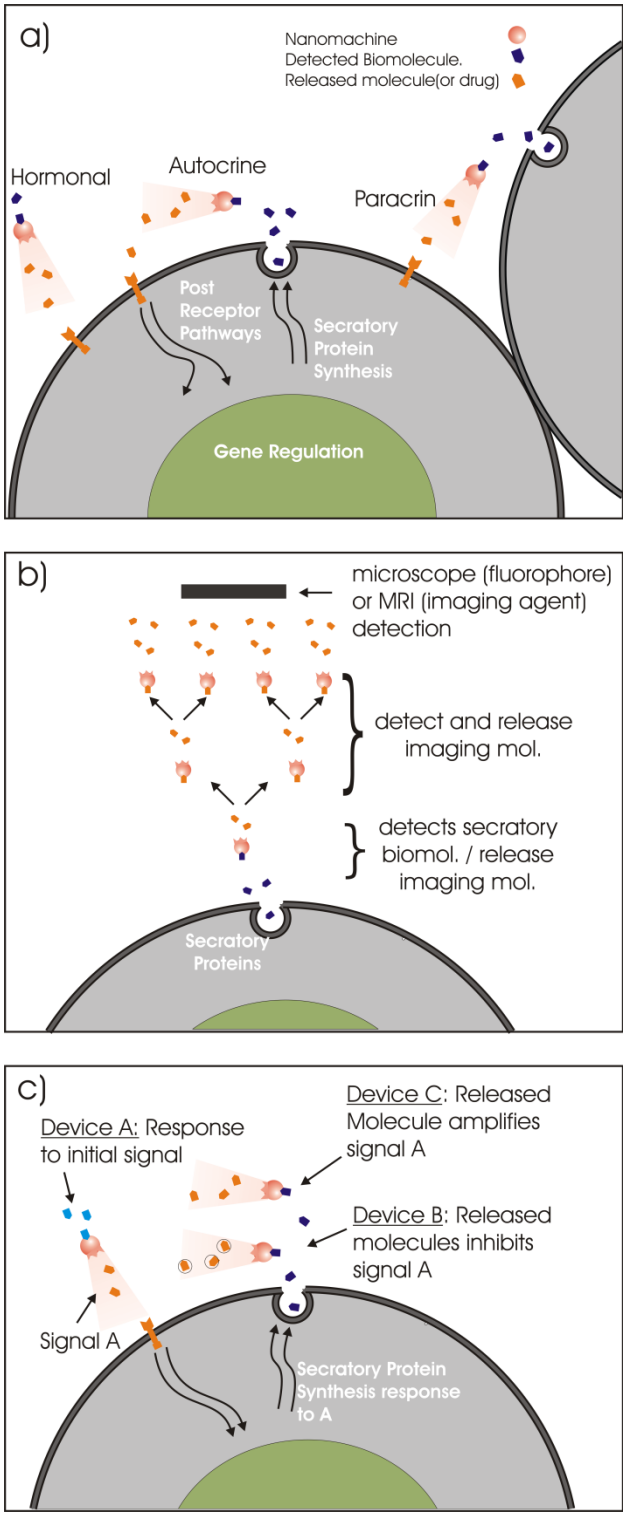

Figure 1.2 Conceptual applications of platform for artificial signal transduction

1.3 Natural Ratchets

Brownian ratchets are a subclass of Brownian machines. They are employed by nature to perform a wide range of tasks including providing propulsion for filopodia protrusion, motion in the bacteria *Listeria monocytogenes* and the translocation of proteins across membranes.[4,5] They are unlike molecular motors which often obtain power from the hydrolysis of ATP and that operate on mechanochemical cycles (e.g. myosin, kinesan). Instead, natural Brownian ratchets are non-cyclic, obtain power through polymerization reactions, and produce directed motion by rectifying random movements with substrate asymmetries.[6,7] A large body of theoretical work has been developed, including kinetic derivations[8] and models of many natural polymerization ratchets.[5] From an engineering perspective, these systems are autonomous, in that the use of energy from polymerization reactions and random thermal inputs enables a system which can operate without an external source of power or control.

Ratchets are not new in science; early thermal physicists speculated on the possibility of ratchet systems. While these early speculations primarily considered pure thermal energy ratchet systems, they brought to light important characteristics that all ratchet systems must possess. In biology the ratchet system was proposed as the underlying mechanism for the model of myosin more than five decades ago. More recently, with the advent of novel microscopy techniques, numerous systems have been characterized. Several of these, including the listeria ratchet and the ratchet implicated in filopodia protrusion are briefly discussed below.[9] These studies provided additional motivations and frameworks in which to analyze the ratcheting phenomena.The natural ratchets systems most closely resemble the devices which are explored in this research and they provide a degree of engineering design sensibility. Numerous theoretical treatments of non natural ratchets exist; from these, ways to predict and characterize the functionality have been introduced.[8,10,11]

1.3.1 Actin Ratchet of Filopodia Protrusion

Initial studies evaluating the extension of the filopodia were conducted by Janmey.[12] He conducted a simple experiment wherein he loaded a liposome with actin monomers and triggered polymerization (Figure 1.3). This experiment demonstrated that the polymerizing actin rod possessed sufficient energy to provide a fingerlike extension against the wall of the spherical liposome. Subsequent analysis was performed by Peskin et al.[5] who through a combination of thermodynamic analysis and molecular dynamic simulation produced predictive models of this protrustion. Peskin began by considering the earlier work of Miyamoto and Hotani where they explored the free energy limitations of the ratcheting filopdia. This analysis looked at the required thermal energy to elongate a lipid cylinder with a radius of 5nm by 50 um. They

asserted that each monomer would be capable of supplying -14 k_BT of thermal energy and that the total energy required for the extension would 2 x 10^4 k_BT.[13] They then concluded that a sufficient number of monomers would be involved in the extension to provide the required energy. Peskin then setup mechanical/diffusion models and arrived at relation velocity of extensions vs. the load force that the ratchet must overcome.

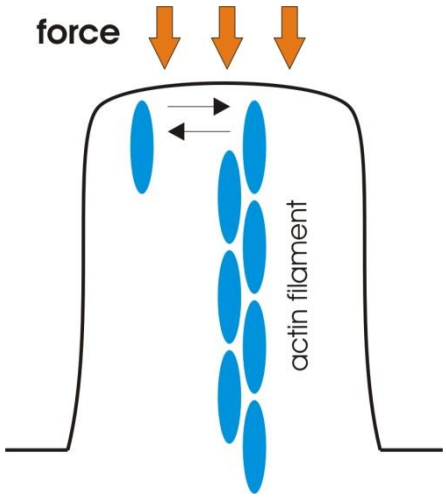

Figure 1.3 Ratchet mechanism of filopodia protrusion.

1.3.2 Lysteria Monocytogenes

The pathogenic bacteria Listeria monocytogenes uses a ratchet to provide propulsion for the bacterium as it moves through the cytoplasm of its host cell. Using florescent photo-activation Theriot et al.[14] observed that Listeria monocytogenes generated a trail of actin fibers oriented in the direction of movement. They observed the insertion of actin monomers into the interface between the trail and the bacterium membrane.

It was subsequently proposed by Peskin et al. that the random thermal movements of the bacterium were rectified by the polymerizing tail.[5] To asses this, they used models of Brownian ratchet movement in conjunction with estimates of the encountered force and the rate of diffusion. They concluded this was indeed a ratchet mechanism and determined it possessed average speeds of around 0.2 um/s for a single actin fiber with a motive force about 9 pN. Beyond this force the ratchet will stall and not progress forward.

1.4 Theoretical Treatments of Ratchets

In conjunction with the multitudes on natural systems, a wealth notional ratchets systems have been investigated. Several excellent reviews of these systems can be found in the literature.[15] This set of these systems contains too many variants list. Nevertheless, all of these contain several hallmarks which help to define them as ratchet systems. Contrasting these systems highlights similarities which allow them to be further categorized and thus theoretically treated with a greater degree of precision.

1.4.1 Breaking Detailed Balance Symmetry

Before discussing the hallmarks of ratchet systems, it is important to note a distinction that can cause problems as result of antiquated nomenclatures. Notional ratchet systems, such Smoluchowski's trap door, are hypothetical systems envisioned to break detailed balance in a system.[16] Detailed balance symmetry states that under equilibrium, flux rates in a system take place in the same proportions in either direction so that no net flux is generated. However

systems like these present a phenomenon currently deemed impossible because they deny the possibility of thermodynamic equilibrium. The ratchet systems described below all require a source of energy. That source may not be obvious but nevertheless it is exists and can come from gradients, the random system input, or as is often the case of natural ratchets systems, from chemical energy.

1.4.2 Physical Hallmarks of Ratchet systems

Brownian ratchet systems invariably produce directed motion on a variable potential energy surface that results from stochastic or forced random perturbations of a system. For this phenomena to occur four characteristics must be present; they include:

a. a randomizing element, which need not be thermal agitation

b. a source of energy (in natural systems this tends to be chemical energy)

c. an asymmetry in the energy landscape along the coordinate of motion

d. a finite energy surface along the coordinate of motion

It is important to note that the nomenclature for ratcheting is inconsistent across research fields. In some, ratchets are not defined as possessing a finite energy surface, while in biology the requirement of a finite energy surface helps to distinguish ratchet systems from molecular motors. Motors can continually produce motion if a source of energy is present. Throughout this thesis and in prior sections we have adapted the definition that requires the surface to be finite.

1.4.3 Classifications of Brownian Ratchet Systems

As noted above, there exists an extremely large diversity of notional ratchet systems, many of which have no clear applicability at the present moment. For this reason, I have greatly limited this discussion to those which are Brownian in nature (e.g. facilitated by fluctuation driven transport). A clear categorization of ratchets has been formulated by Kay et al.[17] Here Kay presents two classifications of fluctuation driven transport ratchets with applications to chemistry and biology in mind; ‘energy ratchets’ which include pulsating and tilting ratchets, and ‘information ratchets’. As Kay notes, both of these categories bias the movement of the Brownian substrate. I discussed each of these below in detail.

1.4.3.1 Pulsating Ratchets

Pulsating ratchets operate by introducing a fluctuation to the energy minima and maxima of a system. The simplest way to envision this type of system is to consider a saw-tooth shape energy landscape where the Brownian particle rests at equilibrium positions dictated by the energy

minima. In this system the energy landscape is cycled off and on, allowing random drift of particles followed by the establishment of a new equilibrium when the potential is turned on.

Because of the shape of the landscape, particles can achieve directed motion. The operation of this ratchet is shown schematically in Figure 1.4. The simple pulsating ratchet discussed above is rarely found in complex systems, instead variations between on and off states is more likely to be complex. In addition, the triggers for these states may not be periodic and may be triggered by a combination of events (e.g. multiple molecular binding events). In Figure 1.5, I show an example of such a system, called a flashing ratchet.

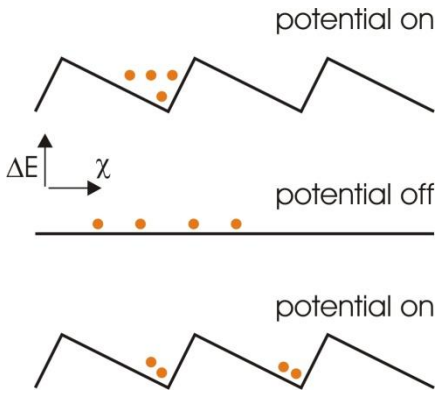

Figure 1.4 Operational Schematic for a simple pulsating ratchet

1.4.3.2 Tilting Ratchets

The tilting ratchet is a form of energy ratchet characterized by constant landscape and a changing random input potential. A simple example of the tilted is a structure with periodic asymmetric energy landscape subjected to a thermal force which moves between two states. This type of ratchet is conceptualized in Figure 1.6; here the Brownian particle experiences a high and low thermal force. At low thermal forces insufficient energy is present to allow the brownian particle to cross the forward and reverse energy barriers.

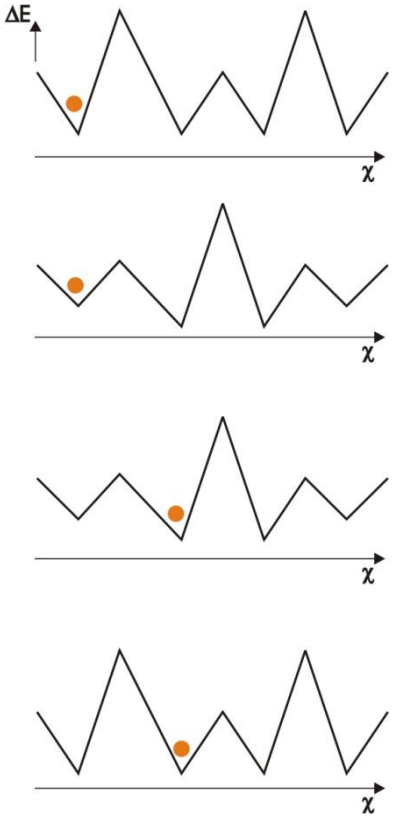

Figure 1.5 Schematic representation of flashing ratchet energy surface

1.4.3.3 Information Ratchets

The information ratchet operates using a different principle than the energy ratchets discussed above, wherein, the potential energy surface or driving random input was varied. Instead, information ratchets operate by changing the potential energy landscape as a function of the Brownian particle position.

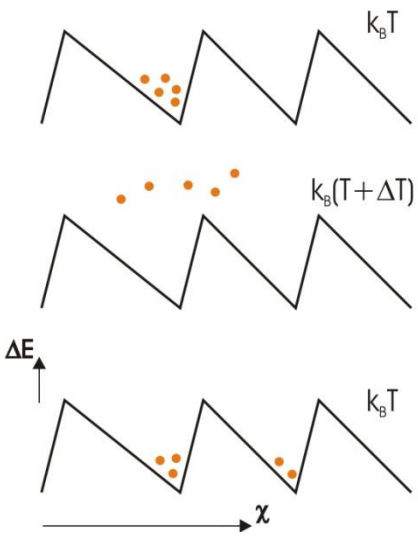

Figure 1.6 Schematic representation of the tilted energy ratchet landscape

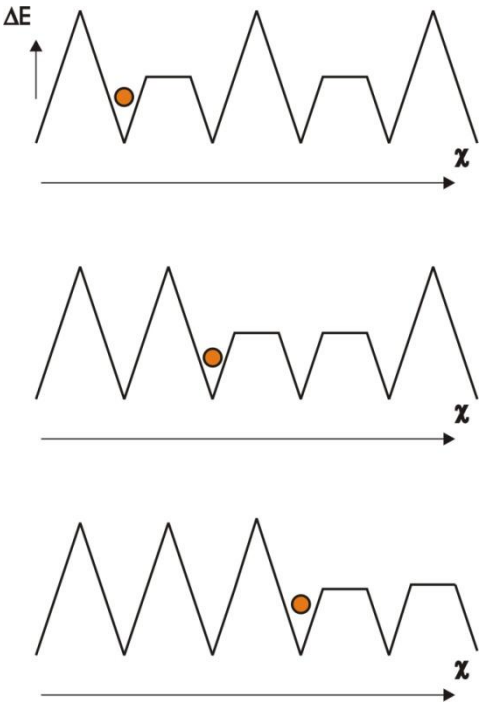

Figure 1.7 Schematic representation of information ratchet energy landscape

Information ratchets can arise in chemical or biological systems in three ways: a localized change to the potential energy surface based on the particle position; a position dependent change to the particle that alters the potential energy surface; or a switching between two periodic potentials as the particles position changes.[17] In physical terms these situations could result from the position dependent initiation of catalytic activity or from a binding event that changes the state of a system.

1.4.3.4 Hybrid Ratchet Systems

Hybrid ratchets are perhaps the most likely to occur in natural systems. In many cases the force applied to a ratchet will change as it progresses along the Brownian particle coordinate. The applied force to the system will inevitably result in a change in the energy landscape. The changing landscape will incorporate elements of information ratchet. The relationship between force and landscape energy is a well known phenomena.[18,19]

The ratchet we have designed and constructed is a form of information ratchet that also contains elements of the flashing ratchet. This connection will become clear in Chapters 2 and 3 where the operational mechanism is discussed.

Chapter 2

Synthetic Brownian Ratchet Design using Lithographically Patterned Nanowires

In this Chapter I discuss the operation and design of a first generation Brownian ratchet system. As noted in Chapter 1, the operational mechanism contains elements of both the flashing ratchet (e.g. a type of pulsating ratchet) and the information ratchet. It is also similar to the polymerization ratchets observed in nature in that power is obtained from molecular bond free energy. This chapter begins with a description of the physical mechanism of operation. Specific details of the thermodynamic and mechanical properties that give rise to the landscape are expanded upon in Chapter 3.

2.1 Mechanism of Operation

I adapted the chemomechanical ratchet strategy to produce a switch that autonomously transduces molecular signals into mechanical deformation/force. In my design antibody-antigen bonding serves as the polymerization reaction. This shift in strategy, where the polymerization species is a sensed molecule, allows the ratchet to become a transducer wherein the detected molecule and power source are one and the same.

The structure of our device is shown in conjunction with the schematic for its mechanism of operation in Figure 2.1. The device is composed of a clip shaped backbone conjugated with a high density layer of polyclonal IgG antibodies (Figure 2.1a, right). For clarity only antibodies in the region relevant to zippering are shown, although it is important to note that on the actual device the entire surface is coated. Prior to encountering a ligand, the device thermally vibrates within a potential well (Figure 2.1a, left) governed by the flexure characteristics of the backbone and temperature of the bath. In the figure, the y-axis represents the change in potential energy, ΔU, which originates from the strain energy in both the backbone and any stretched molecular complex. The x-axis represents the position of the ratchet along a Brownian coordinate. I have defined this coordinate as a measure of ratchet closing, specifically the net movement of the tips of the switch. As an aside, the average amplitude of the thermal vibrations is described by the equipartition theorem. More precise analytical formulae can be used to compute the vibration frequency response for simple geometries considering the effects of viscous medium and shape.[20,21] These models have been shown to be very accurate and were derived with applications to atomic force microscopy in mind although they are relevant to predicting the dynamic response of the simple nanowire ratchet under forced or thermal vibrations as well.

The transition between states X_1 and X_2 (notation $X_{1\text{-}2}$) requires that the random vibration energy input be capable of surmounting the forward energy barrier, $U_{1,for}$, and that a bound/unbound configuration exists between opposing receptors (Figure 2.1c, I). Upon the transition (i.e. first complex formation, Figure 1c, III) a new potential well (Figure 2.1b, left) is established, with the equilibrium position advanced in the closing direction, χ, and bound by a new reverse, $U_{2,rev}$, and forward, $U_{2,for}$, barrier. The power for each of these transitions is

extracted from the ligand-receptor binding free energy, ΔG_b, during the simultaneous relaxation of the backbone and tensioning of the complex (Figure 2.1c). The conversion of free energy to mechanical work during molecular tensioning is accounted for in the Gibbs free energy equation.[19,22] The transitions between states continue until the zipper is closed (Figure 2.1d).

Obtaining this functionality described above is dependent on the device topology as well as the thermodynamic and mechanical properties of both the backbone and bond complex. In order to estimate the proper thermodynamic characteristics for the complex, backbone size, shape and material that give rise to viable mechanical properties we created a model that provided us estimates of the energy landscapes. We then examined the heights of the forward and reverse energy barriers in relation to the IgG bond energy and the magnitude random vibration input. Further, we assessed the bonds provided sufficient force and energy to allow the phenomena to occur. After manually exploring various cross-sections, interior angles, elastic moduli and IgG receptor spacings we chose a configuration that had the potential to operate as a Brownian ratchet. Descriptions of the models are provided in Chapter 3.

2.2 Device composition

Based on the model estimates, I selected a gold switch shaped device measuring 50 nm in width, 30 nm thick and with an interior angle of 6º (Figure 2.2). The device is anchored by a small metal bridge and suspended ~350 nm above the substrate to allow freedom of movement. Two device sets were produced with arm lengths, l_w, of 1 μm and 2 μm. I selected a polyclonal immunoglobulin G (IgG) (rabbit anti-streptavidin, GenScript Corporation) molecule as the receptor in order to demonstrate the versatility of the transduction and because of its known inherent flexibility.[23] This flexibility increased the probability of complex formation, especially in the cases where the IgG molecules on opposing arms were misaligned.

I also sought to maximize the functional density of active antibodies on the nanowire surface in order to minimize forward energy barriers. Closely spaced complexes reduce the distance (along χ in Figure 2.1) between state transitions. In physical terms, this reduces the vibration amplitude required to bring the receptor and receptor-ligand complex into proximity for sandwich bond formation. I chose a conjugation technique that had been shown to achieve a uniform, stable and sterically accessible antibody layer with a high active density.[24] This technique uses a crosslinker, Dithio-bis(Succinimidyl Propionate) (DSP), to bind Protein A (Recombinant Staphylococcal) (PrA) to the gold backbone. DSP is a homobifunctional crosslinker molecule which binds to PrA via the amine residues – at neutral pH or higher – and to the gold surface via the sulfide exposed during cleaving in DMSO.[25] PrA then binds specifically to the Fc region of IgG resulting in an oriented molecule and a reduction in the loss of specific binding competence. This method compared favorably with others in the literature[26-28] and provided the necessary covalent conjugation. Non-covalent techniques, while simpler, can

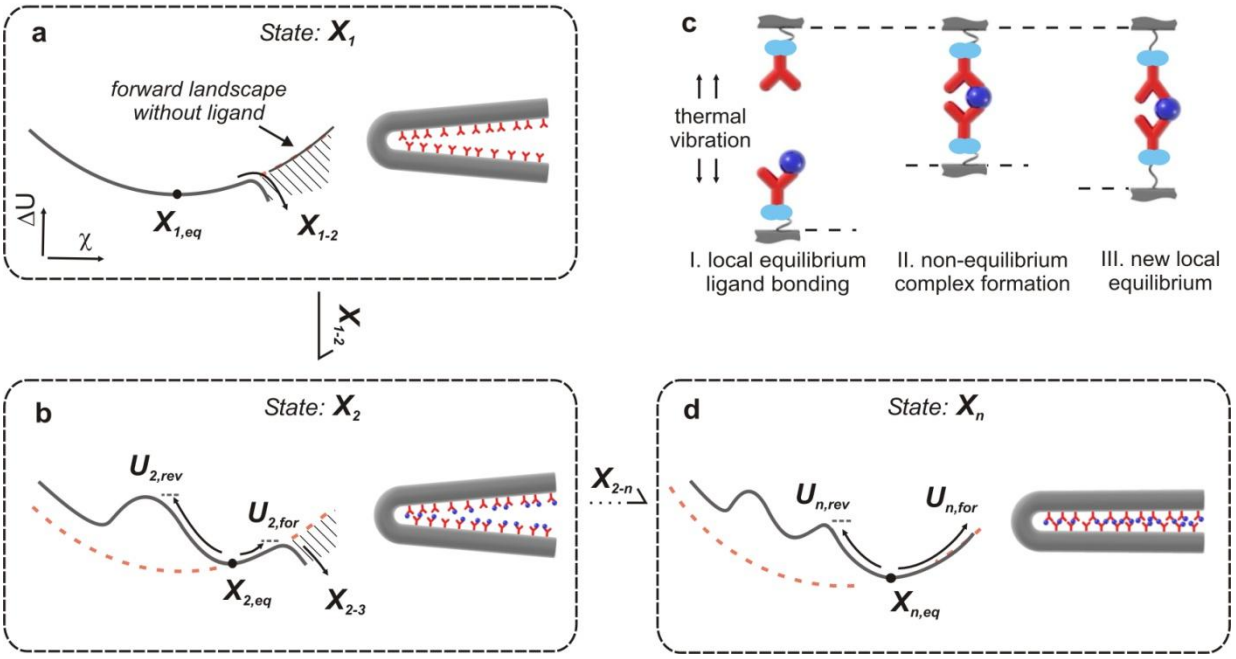

Figure 2.1 Physical mechanism of *Brownian ratchet* type chemomechanical transduction. In this depiction, the structural backbone is shown in grey, antibodies are shown in red, and the sensed molecule is shown in dark blue. (a) Energy landscape and switch configuration for State X_1 , prior to encountering a ligand (b) State X_2 , during ratcheting and (d) State X_n, closed configuration (c) The equilibrium transition between states is caused by the formation of new antibody-antigen-antibody sandwich bond.

result in decoupling under high force. The conjugation method and characterization of receptor molecule densities is provided in Section 2.3.2

Measurements of the IgG density using this technique on an evaporated gold substrate were taken using immune-SEM. In figure 2.2b these are shown at the same size scale as the device image (figure 2.2a). The nanogold labels (18 nm, Nanoprobes) provide some sensibility of the expected IgG density on the device surface. Here, the larger size of the immunogold label (IgG + gnp) produced results that are a conservative estimate of the density.[29] To confirm the density of active sites I took measurements of the density of streptavidin bound to IgG under identical conditions used in the experiments. These are shown in Figure 2d and are similar to the coupled IgG density, thus confirming a high degree of oriented molecules.

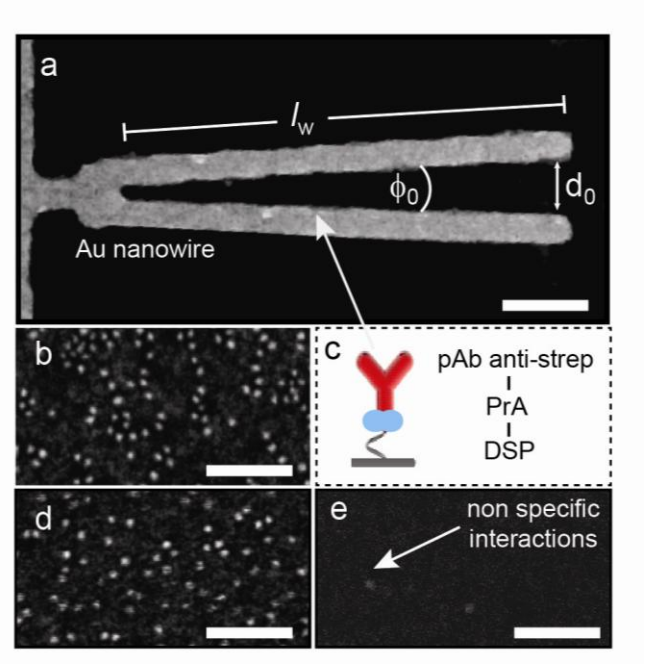

Figure 2.2 Device topology as tested. All scales are 200 nm (a) device backbone diagram top view (b) Immuno-SEM showing the surface density of IgG molecules. (c) receptor complex molecular components (d) Immuno-SEM of the active IgG density (e) Immuno-SEM of the non-specific interations of strptavidin with the functional surface

Background images to confirm the minimal effect of non-specific interactions was measured on a 1% BSA blocked surface to ensure they did not contribute to ratcheting (Figure 2.2e). A detailed discussion of the functional surface characterization is given in Section 2.4. Before functionalization, micrographs of critically point dried devices were captured. The angles were manually measured and later served as a baseline for the response. A slight variation of angles existed as a result of residual stress and the lithographic resolution of the process (Figure 2.3). The mean and distribution of angles for the 1 μm ($\mu = 5.22^{\circ}$) and 2 μm ($\mu = 5.96^{\circ}$) instantiations were well within our desired tolerance to produce a pronounced device response.

2.3 Device Fabrication

As noted, fabrication of the device was conducted in series of two steps, beginning with the creation of the gold structural backbone and followed by conjugation of the receptor molecules. Between these steps, all devices were imaged and subsequently stored in an aqueous solution to prevent the possibility of stiction forces bonding the arms of the device.

2.3.1 Gold Backbone

Devices were fabricated on silicon wafers. The wafers were first coated with poly-germanium layer via sputtering (350 nm, R_{rms} < 2nm). A resist bilayer (PMMA A2-950k/A3-50k, 40nm/70nm, Microchem) was then deposited by spin coating and patterned using electron beam lithography (Crestec CABL-9510CC High Resolution Electron Beam Lithography System) and developed (MIBK/IPA 1:3, Microchem) for 60s at room temperature. Subsequently, a Cr/Au (5nm/30nm) metal layer was directionally deposited by electron beam evaporation. Metal liftoff was then performed in acetone at room temperature. This resulted in devices anchored to the poly-germanium layer. The devices were then released by under-etching the poly-germanium layer in 10% H_2O_2 for ten minutes at room temperature. A schematic of this process is shown in Figure 2.4.

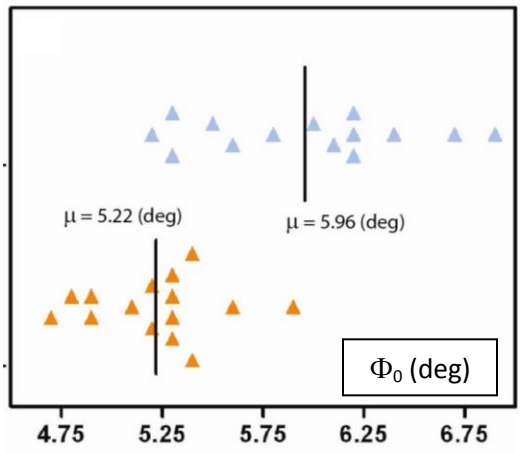

Figure 2.3 Process variation of initial interior angles for 1 um (bottom, orange) and 2 um (top, blue) devices

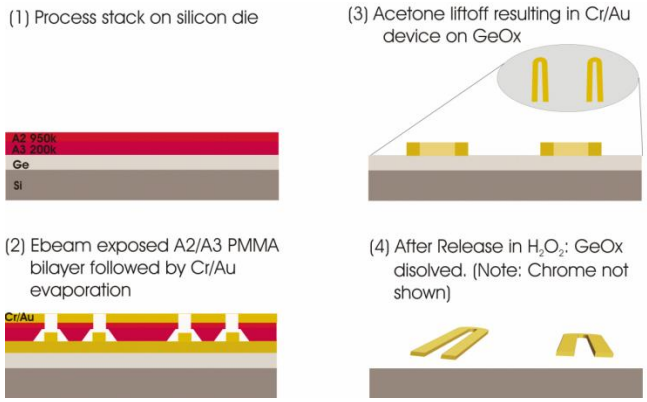

Figure 2.4 Device Fabrication process flow for the construction of gold backbone. The device anchor to the substrate is not shown.

2.3.2 Functionalization Protocol

After creating the gold structural backbone, the devices were washed in acetone (3x, 5min) then in DI (3x, 5 min). The DI was then replaced by the organic solvent Dimethyl sulfoxide **(**DMSO) though a series of three washing steps. A 0.002M Dithio-bis(Succinimidyl Propionate) (DSP) in DMSO solution was prepared. DSP is a homobifunctional crosslinker molecule which binds to Protein A (Recombinant Staphylococcal) via the amine residues – at neutral pH or higher – and to the gold surface via the sulfide exposed during cleaving in DMSO. The solution containing the devices was then combined with a DSP solution and incubated for 2 hrs at room temperature. Unbound DSP was removed from the solution by washing (3x, 5min) in phosphate buffered saline pH 7.4 (PBS 7.4). A solution containing 0.1 mg/ml to 0.5 mg/ml of polyclonal IgG (rabbit

anti-streptavidin, GenScript Corporation) was prepared, and added to the solution containing the devices and incubated for 1 hr at room temperature. Unbound IgG was removed through a series of three washing steps in PBS. BSA (1% in PBS) was then added to the solution to block residual reactive sites and incubated for 1 hr. This method produced an oriented and densely packed polyclonal IgG layer. A high active IgG density was critical to proper device function.

2.4 Characterization of Functional Surface

Two conjugation methods were initially explored; the first method directly cross-linked the IgG to the DSP monolayer, while the second method made use of the Protein A (Pr A) intermediate layer to orient the antibodies, as described above. The results quantifying the active IgG density for both methods (Table 2.1) were obtained using Immuno-SEM. The abbreviations in the table are as follows: Ag is streptavidin, GNP is gold nanoparticle, pAB is polyclonal antibody, AS is anti-streptavidin, and GAR is goat anti-rabbit. In this study all secondary labels were purchased from Nanoprobes (18nm). In Figure 2.5, the raw data is presented; scale bars are all 200 nm.

2.5 Ratcheting Response Results

In parallel, a set of functionalized devices were prepared to be used as active devices and controls. All experiments were carried out at room temperature. All devices began immersed in 1x phosphate buffered saline (PBS) (pH 7.4, 25°C). For the active devices we adjusted the concentration of tetravalent streptavidin to 1.67 μM, while in the controls a dummy aliquot containing only 1x PBS was introduced. Both device sets were then incubated for 30 minutes. Following incubation, all devices were washed in DI (3x) to remove both salts and residual streptavidin. Both active and control device devices were then fixed in a 2% solution of glutaraldehyde for 30 minutes. The fixation agent was then removed in a series of washing steps, first in PBS 7.4 (3x, 5min), then in DI (3x, 5min). The devices were then re-suspended in methanol in a through a washing sequence (25%, 50%, 100% methanol) and critically point dried (Tousimis 915B Critical Point Dryer).

Electron micrographs of the device response are shown in Figure 2.6. The response between active and control devices is clearly distinguishable. No devices were observed with the arms completely sealed as would occur if stiction forces had been present. In addition, the separation of arms was often approximately the length of the sandwich bond, as can be seen in figure 2.6b. In Figure 2.7 we contrast the active and control response. The response is normalized in terms of the percentage of movement toward a closed state, C_r. We define a closed state as the point at which the device tips are 38 nm apart, which is the approximate physical length of the sandwich bond complex (varies with orientation). The definition of C_r is then: $Cr = d_f / d_0 - h_c \times 100$. A clear difference is seen between the median for the control (C_r = 16%) and for the active (C_r = 86%) devices. For the active devices (n=11), five devices were observed within 10% of a

Sample	Functionalization Method	Detection Method	Particles/cm^2	Ave. Spacing [nm]
1	DSP (1mg/ml), pAb (1mg/ml)	GNP (18nm) GAR (0.5ml/ml)	1401	40.2
2	DSP(1mg/ml), pAb (1mg/ml)	Ag (1mg/ml), pAb (1mg/ml), GNP AS (0.5mg/ml)	690	57.4
3	DSP (1mg/ml), PrA (0.5mg/ml), pAb (1mg/ml)	GNP (18nm) GAR (0.5ml/ml)	1064	46.2
4	DSP (1mg/ml), PrA (0.5mg/ml), pAb (1mg/ml)	Ag (1mg/ml), pAb (1mg/ml), GNP AS (0.5mg/ml)	1156	44.3
5	DSP (1mg/ml), PrA (0.5mg/ml)	GNP (18nm) AS (0.5ml/ml)	11	456.0

Table 2.1 Functional densities obtained using various conjugation methods

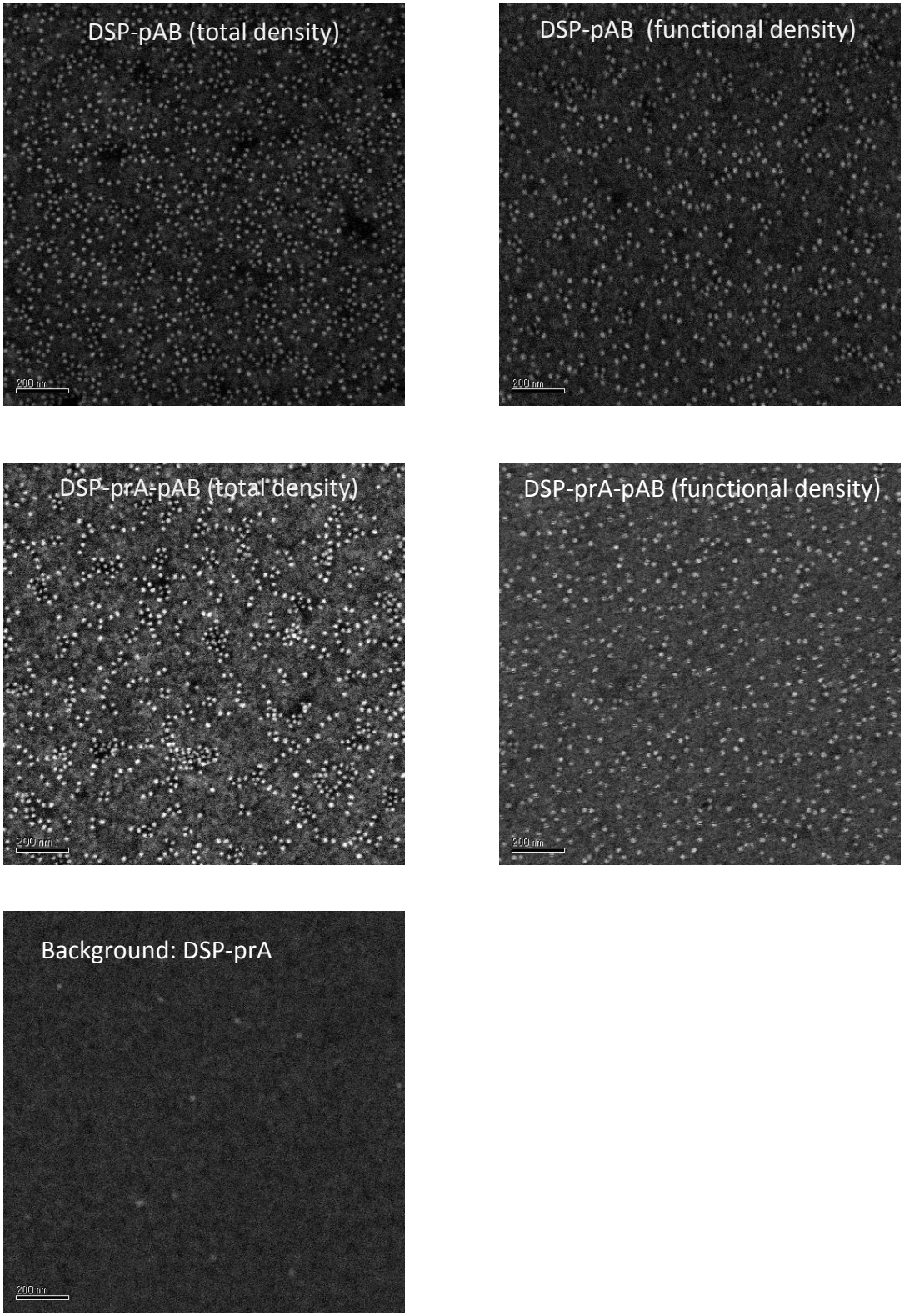

Figure 2.5 Functional densities obtained using various methods

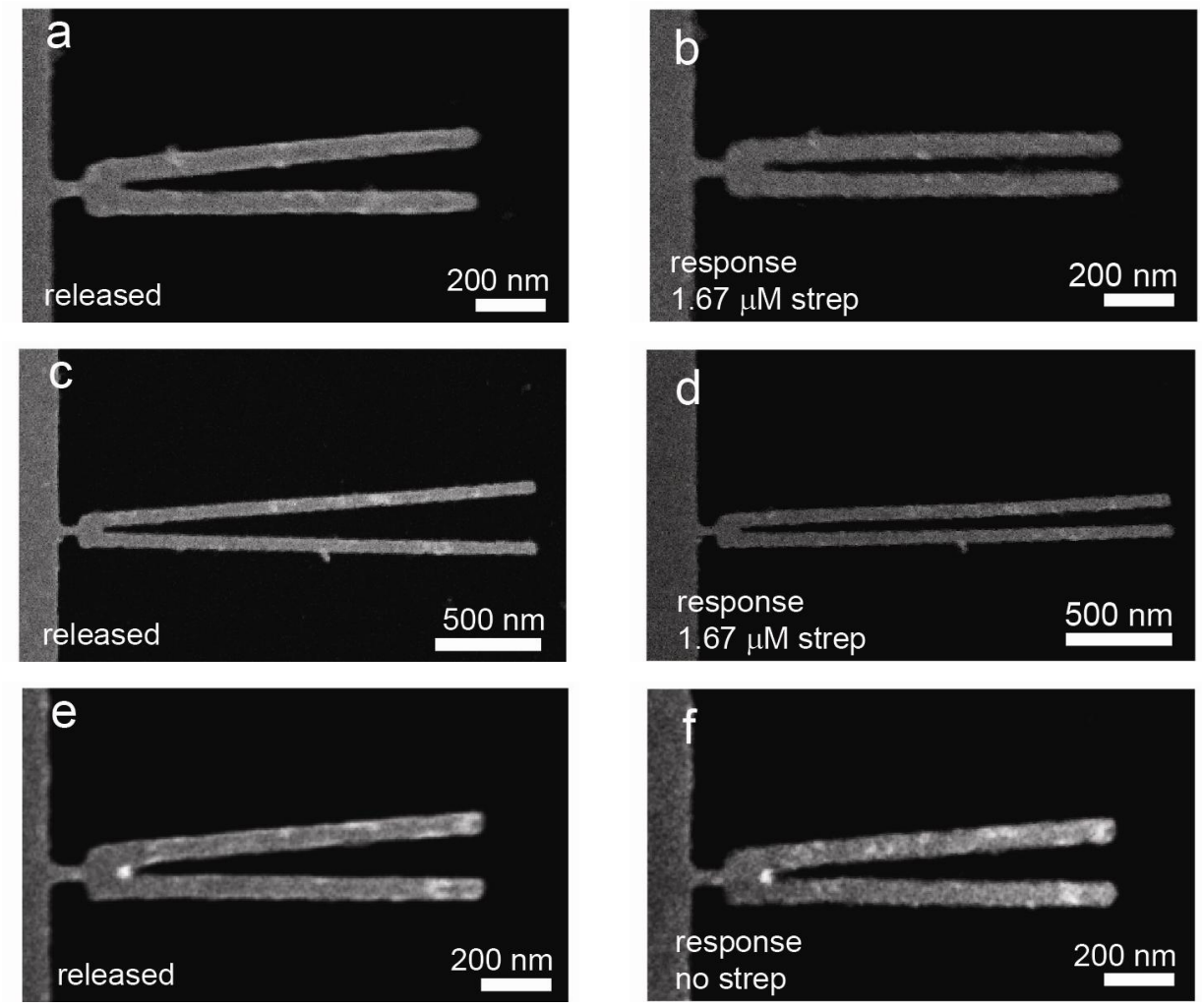

Figure 2.6 Electron micrographs of 1um and 2um device response to 1.67μM of strepatavidin as well as the control response (T = 25ºC, t = 30 min) .

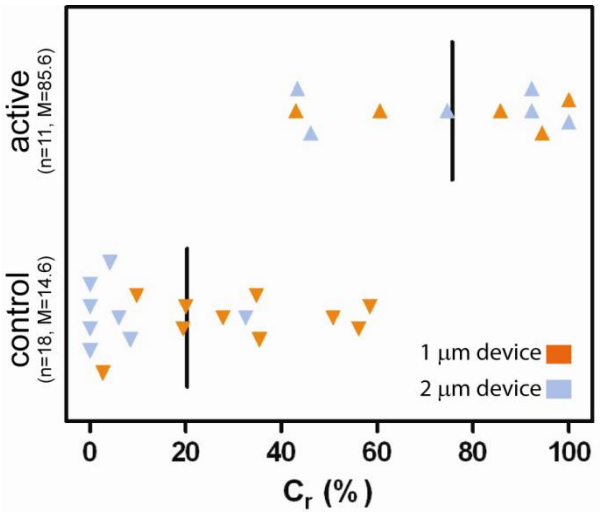

Figure 2.7 Control and active device response mean and distribution in terms of percent movement toward closed state, Cr

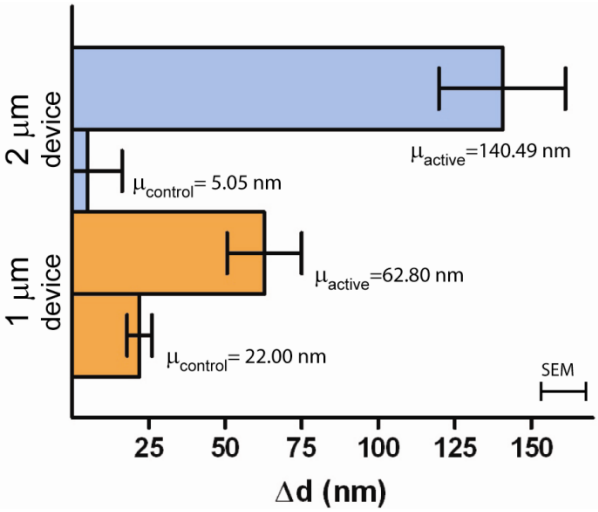

Figure 2.8 Control and active device response mean and variance in terms of amount of tip movement toward the closed state.

completely closed state and no device remained opened. While, in the control sample (n=18), eight devices were observed within 10% of a completely open state. In Figure 2.8 we decompose the net displacement of the tip, Δd, for the 1um long active (μ=62.80 nm); 1um long active control (μ=22.00 nm); 2 um long active (μ=140.49 nm); and 2 um long control (μ=5.05 nm).

2.6 Conclusions

In this chapter I provided evidence demonstrating how a simple architecture, composed of antibodies and a lithographically patterned nanowire, can elicit a chemomechanical response to a user specified ligand. As the ability to more precisely control the fabrication of the structural components increases and methods for site specific functionalization evolve, the advent of Brownian ratcheting as a fundamental approach becomes more interesting. Recent progress in both highly controllable self-assembly methods, such as DNA-origami present opportunities to further investigate the ratcheting mechanism and adapt it to technological uses. In the following chapter I theoretically address the likelihood of ratcheting for a given design. In Chapter 4, I utilize both the theoretical analysis from Chapter 3 and the methods of self-assembly to create the second generation devices hinted at above.

Chapter 3

Modeling and Simulating the Brownian Ratchet Energy Landscape

3.1 Introduction

In this chapter the physical models and simulations for the Brownian ratchet are presented. The simulations were created using both data from molecular dynamic simulations, generated by external labs, as well as, finite element models generated in-house. These simulations estimate the interchange of bond energy with the backbone and bond complexes. The external data is primarily in the form of force-displacement and force-bond energy relationships. Resultant energy landscapes of two designs are presented. These stiffness and shape of these designs are similar to what would be expected for the self-assembled DNA based device discussed in Chapter 4.

3.2 Potential Energy Landscapes

Successfully designing a Brownian ratchet requires that rectified motion is both energetically feasible and statistically favored in the closing direction (χ increasing, Figure 3.1). To evaluate these criteria we construct a quasi-static equilibrium model to compute the potential energy pathway for the first vibration mode of the backbone. The total potential energy, U_{total}, is the sum of the both the strain energy contained in the backbone, U_s, and the total change of potential in the complexes, U_c. All of these terms are functions of the state of the system, X (i.e. the current number of complexes formed), and the Brownian particle coordinate, χ. In the previous chapter, we defined χ as a measure of the degree to which the zipper was closed. For the remainder of this chapter we apply the specific definition of χ depicted in Fig. 3.2a. For a given set of formed sandwich bond complexes, $\{z_{1\ldots}z_Q\}$, the change in potential along χ is given by:

$$\Delta U_{total}(X,\chi) = U_s(X,\chi) + \sum_{p=1}^{Q} \Delta U_{c,p}(X,\chi) \qquad (1)$$

The value of U_s for a given state, X, and *Brownian* particle position, χ, can be computed using finite element analysis for relatively homogenous materials or using molecular dynamics simulation (MDS) for more complex assemblies, such as the self-assembled DNA motifs. In my work I used finite element simulations in COMSOL.

Computing the *change* in potential of the complex, U_c, for a given state is more involved. Under quasi static equilibrium conditions, each stretched receptor-ligand bond has a free binding energy change, ΔG_b, between a bound and unbound configuration given as[22]:

$$\Delta G_b(F) = \Delta G_b{}^0 + k_B T \ln\frac{[S]}{[C]} - \int_{r=0}^{r_1} F dr_1 \qquad (2)$$

where ΔG_b^0, is the standard state free energy, r represents the force-extension reaction coordinate of the bond, k_B is Boltzmann's constant, T is the bath temperature and F the total force applied. Here, the activities *[S]* and *[C]* represent the probability of the system occupying a bound and unbound configuration, while in conventional bulk experiments; *[S]* and *[C]* represent the concentrations of the ligands and receptors. The initial change in $U_{c,p}$ upon bonding (equal to $\Delta G_b(F=0)$) therefore increases as force is applied (e.g the complex is stretched). Note that ΔG_b is a negative quantity and the direction of F is negative during stretching. As an aside, the total worked performed stretching the set complexes $\{z_1..z_Q\}$ is equivalent to the work performed on the system, W, which can be divided by the total binding free energy supplied, $Q{\cdot}\Delta G_b(F=0)$, to give an estimate of the efficiency. During movement along χ, changes in potential resulting from intramolecular stretching also occur, with each molecule in the complex contributing to the total change in potential. For the complex depicted in Fig. 2b, the work performed is:

$$\int_{r=0}^{r} F dr = 2\int_{r_2=0}^{r_2} F dr_2 + 2\int_{r_3=0}^{r_3} F dr_3 + \int_{r_4=0}^{r_4} F dr_4 \qquad (3)$$

where, r_2, r_3 and r_4 are the force-extension reaction coordinates for the linker, receptor and ligand respectively.

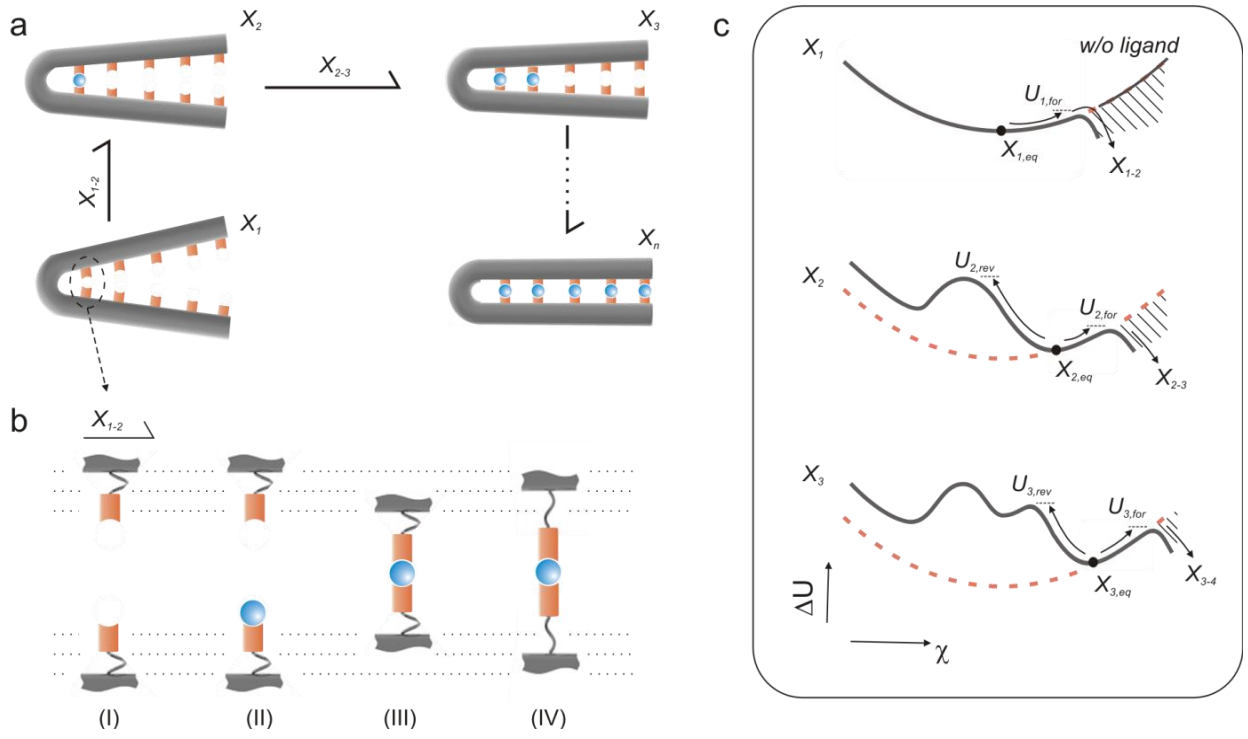

Figure 3.1 Schematic of device operation. (a) operational overview (b) state transition at an individual receptor-ligand pair. (c) notional energy landscape for three states, where the coordinate, ΔU, represents the relative changes in potential energy and χ, the Brownian particle coordinate, which is a measure of the degree to which the device is closed.

The total change in the potential energy of then system is then sum of all intramolecular and intermolecular contributions:

$$\Delta U_c(F) = 2\Delta G_b(F) + \int_{r=0}^{r} F dr \quad (4)$$

The stretched complex is analogous to a nonlinear, non-monotonic spring formed by the series of intermolecular bonds and molecules (Fig. 3.2b, right). Within this series, energy is partitioned as a function of the relative stiffness of the individual components, with very rigid bonds absorbing insignificant amounts of energy. This characteristic allows us to neglect intermolecular covalent bonds (as in Eq. (3)) and molecules with a high relative stiffness. For example, if the linker molecules are significantly less stiff than the intramolecular stiffness of the ligand and receptor we can further simplify Eq. (3) by neglecting the second and third terms. We note that, Eq. (4) is not defined as function of χ, and that relationship between χ, F and r must be resolved using finite element simulations after obtaining the complex force-extension profiles and establishing a design for the backbone. The shape and magnitude of the force-extension profiles in Eq. (3) are unique for every molecule. For polymers that can be represented as freely jointed or wormlike chains, well-known models exist[30,31] and for several molecules with widespread practical importance, profiles have been obtained by force probe atomic force microscopy (FPAFM).[32] The unbinding profiles of the complex intermolecular bonds in Eq. (2) cannot be readily obtained. FPAFM methods fail in part because the force cannot be resolved across the extremely

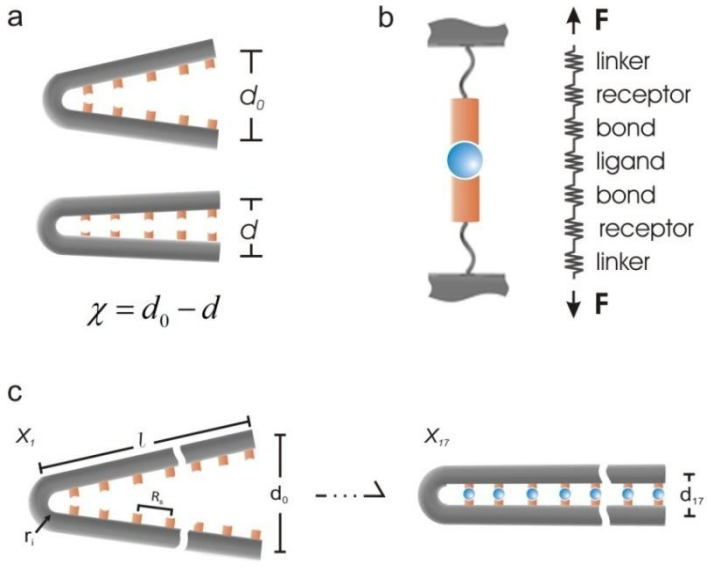

Figure 3.2 Definitions (a) Brownian particle coordinate, χ, in terms of the initial opening, d_0, and current opening, d (b) diagram of sandwich bond complex used in the simulation, left, and analogous series spring model for the complex, right (c) model geometric parameters

small length scales of the reaction coordinate, which are often less than 5 Å. Nevertheless, the unbinding force, length of the reaction coordinate[33-35], and their relationship to loading rate can be addressed.[36] In addition, the practical importance of understanding atomistic mechanisms of ligand binding has led to the use of steered molecular dynamics (SMD) to simulate FPAFM experiments. Here, force-extension profiles can be obtained but at sub microsecond timescales, much faster than would be encountered during stretching in the zipper. However, with the wealth of information obtained from MDS in conjunction with data obtained from AFM useful force-extension profiles can be constructed for zipper design.

3.3 Quasi-Static Equilibrium Models

To assess the feasibility and to elucidate the design constraints of zippers we again consider the prototypical zipper design shown in Fig. 3.1. Geometric definitions are shown in Fig. 3.2c and simulation parameters are summarized in Table 1.

For the complex, we selected a Poly(ethylene-glycol) linker, an Fv fragment (anti-lysozyme) as the receptor and an antigen as the ligand (lysozyme). These components are widely used in bio-sensing and single molecule experiments and thus thermodynamic and mechanical properties are readily available. With IgG fragments the chemomechanical response can be tailored to a vast number of sensed molecules (antigens). In our model, we have applied the assumption that both the receptor and ligand are significantly more rigid than the linker molecule and the complex bond. For the selected molecules this is a good assumption; the stiffness of globular proteins (lysozyme) and Fv fragments (anti-lysozyme) in their native state are significantly higher than the PEG linker and complex bond. To obtain a solution, force-extension profiles are required for the bond and linker. For the linker, the profile for PEG in water has been shown to be accurately modeled by a Markovian two-level system[37].

$$L(F) = N_s \left(\frac{L_{planar}}{e^{-\Delta G_p / k_B T} + 1} + \frac{L_{helical}}{e^{\Delta G_p / k_B T} + 1} \right) \cdot \left(\coth\left(\frac{F \cdot L_K}{k_B T} \right) - \frac{k_B T}{F \cdot L_K} \right) + N_S \frac{F}{K_s} \quad (5)$$

where N_s is the number of segments, L_{planar} (3.58 Å) and $L_{helical}$ (2.8 Å) are the monomer lengths in their planar (ttt) and helical (ttg) conformation, k_B is Boltzmann's constant, T is the simulation temperature, L_k is the Kuhn length (7 Å), ΔG_p is free energy difference between the helical and planar conformation (3 k_BT), and K_s is the segment elasticity (150 N/m). Additional supporting experiments can be found in the literature.[38]

Resultant force-extension profiles are shown in Fig. 3.3a for three values of N_s. We used a linker with four segments in our primary study and later used shorter and longer linkers to assess the effect of linker stiffness. Rigid short linkers are advantageous in the sense that they reduce the amount of energy that is coupled to complex-stretching, and thus more energy can be transferred

to the backbone. At infinitely high rigidities the linker is not capable of absorbing a significant portion of energy from the bond. While as can be imagined extremely flexible linkers (along the force coordinate) would absorb nearly all of the energy. This would result in stretching of the complex with little energy transferred to the backbone for motion.

Table 3.1. Simulation Parameters

Param	Description	Value	Units
ΔG_0	binding free energy for receptor-ligand pair	-42	KJ mol^{-1}
F_{unbind}	receptor-ligand unbinding force	65	pN
k_b	backbone stiffness at l	4,40	pN/nm
T	Temperature	300	K
l	length	125	nm
Rs	ligand-receptor spacing along l	10,20	"
r_i	internal radius of zipper	7	"
Θ_i	Internal angle	15	deg

The force-extension profile we used for the receptor-ligand bond was drawn from data for the Fv fragment-lysozyme interaction. For this interaction FPAFM experiments have shown an unbinding force of ~65 pN[39] and SMD simulations have been used to produce a detailed force-extension curve at nanosecond timescales. [35,40] As noted above the exact profile is not currently possible at timescales relevant to the zipper. The profile in Fig. 3.3b was thus constructed by using the dominant features and reaction coordinate length from the SMD profile with and the unbinding force magnitudes determined by FPAFM. We believe this notional force-extension profile contains sufficient information for initial zipper designs. The aggregate profile is shown in Fig. 3.3c and the integral was used as a solution to Eq. (4) in the simulation. Note that the non-monotonic nature of the bond produces bifurcations under the quasi static equilibrium assumption. These bifurcations do not exist in real world systems and were used as inputs. Our rational for this was that they had only a minimal effect on resultant energy landscapes. We assessed this by performing perturbations around the bifurcations and visually inspecting the landscapes for noticeable differences.

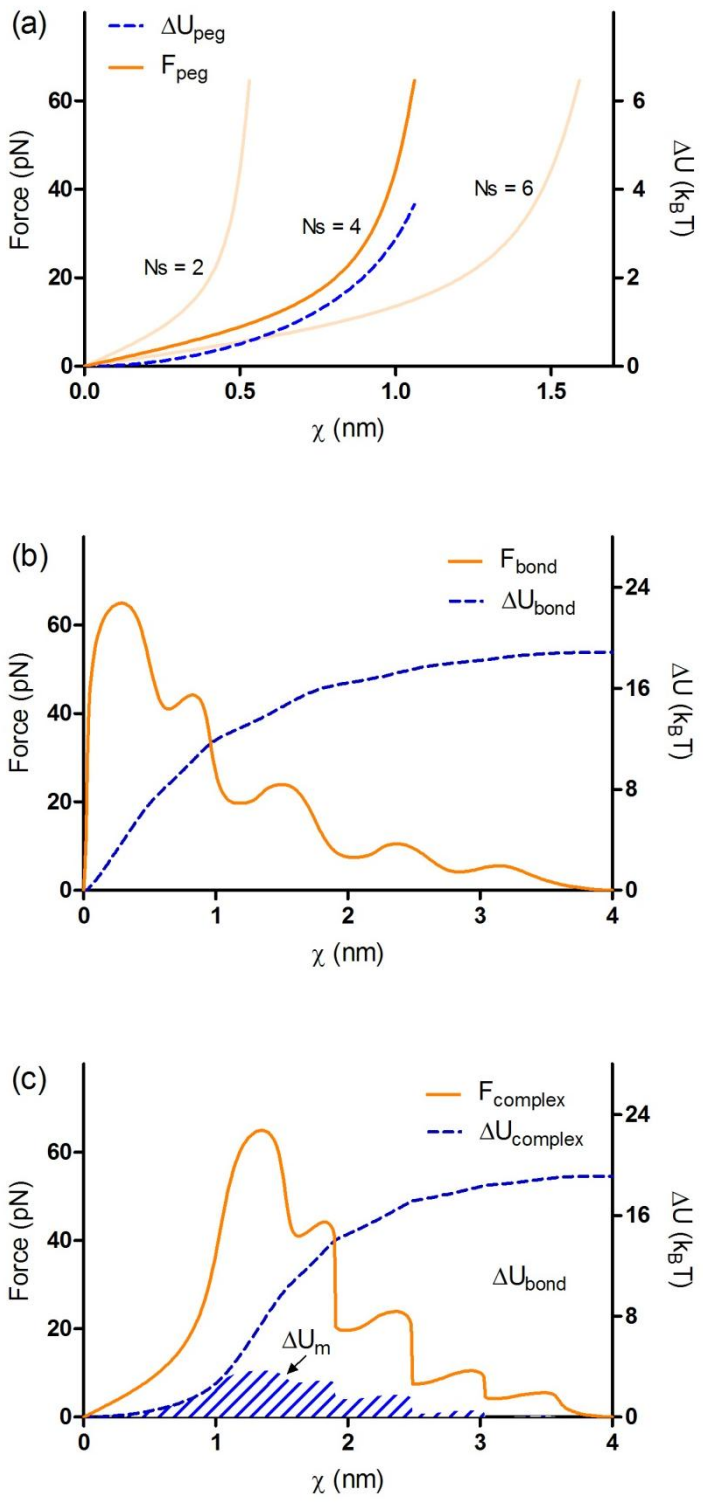

Figure 3.3 Force-extension and energy-extension curves used in the simulation for the (a) PEG linker molecule with N_s = 2, 4 and 6 (b) receptor-ligand bond and (c) the full complex.

3.4 Results and Simulation

Simulations were performed using COMSOL Multiphysics and MATLAB. For a given deformation of the backbone, MATLAB functions were called from COMSOL to provide points on the aggregate force-extension curve. This allowed COMSOL to iterate through changes in the state of the system (e.g. number complex bonds). In Fig. 3.4 we show the energy landscapes obtained for a zipper with a flexural backbone stiffness, k_b, of 0.4 pN/nm (at l = 125 nm). This is a reasonable stiffness for a DNA nanostructure, such as those we created in Chapter 4 using the honeycomb-replete origami technique[41] or alternatively, a soft polymer with a cross-sectional area on the order of 10 nm^2 to 200 nm^2 (depending on elastic modulus and shape). Shown in the figure are the energy landscapes for the states X_1 to X_4 and the states X_8 to X_{11}. The graph shows the change in potential for each state as function of χ. The states transitions are marked by changes in the equilibrium position. For example in $X_{2\text{-}3}$ the equilibrium position moves by 4.62 nm (from a position of 0.57 nm to 5.19 nm). As more bonds form, the movement between states becomes progressively becomes smaller, reducing to net displacements of 0.7 nm in $X_{10\text{-}11}$. This is a consequence of the shape of the zipper and the constant spacing of receptors along the backbone. Another artifact of topology is that the forward energy barrier gradually increases, reaching a maximum at X_4, of 1.54 k_BT then progressively decreasing as is seen in states X_8 to $X_{11.}$

3.4 Beam dynamics

Using models developed by Eysden et al.[21] for resonating nanomechanical beams in water, the number of binding opportunities per second can be computed as a function of the required coupled thermal energy for beams of varying size and stiffness. While these equations neglect the influence of the hinge and treat the structure as a fixed-free beam, they do provide some design sensibility as the hinge region contributes little to the overall flexibility. However the deeper question; which is 'how often will receptor and ligand bind?' can only be answered by relating the structural dynamics to the binding kinetics. This is a far more complex question that can currently only be addressed experimentally. However, it may be possible to create hybrid simulations that use FPMDS, MDS and a lower fidelity mechanics model of the backbone to address this problem computationally. This may be the subject of future work. If we look at the landscapes of a stiffer zipper topology in Figure 3.5, with a k_b equal to 2 pN/nm (at l = 125 nm), and contrast that to the data in Figure 3.4, it is evident that the stiffer geometries require higher thermal energies to cross subsequent energy barriers. The opportunity to surmount the barrier at X_n will happen rarely. However, these more rigid designs might still present candidates for new devices where the random input is not thermal (i.e. the random mechanical excitations are triggered through the bath). Another important consideration is that a rigid backbone and a very soft complex result in a deep potential well. This highlights an important consideration: if severe differences in the stiffness exist, the forward energy barrier may become insurmountable. The complex stiffness must therefore be tuned in agreement with the stiffness of the backbone.

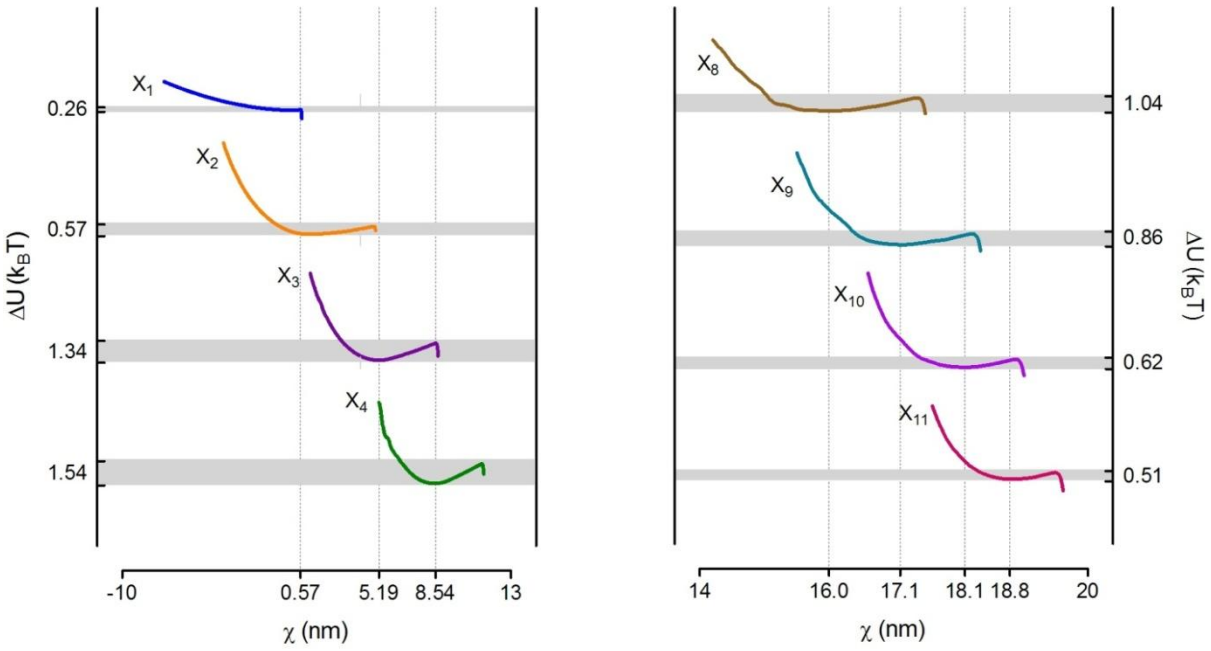

Fig 3.4. Energy landscapes for the prototypical design with a backbone flexural rigidity of 0.4 pN/nm, states X_1 to X_4 (left) and states X_8 to X_{11} (right)

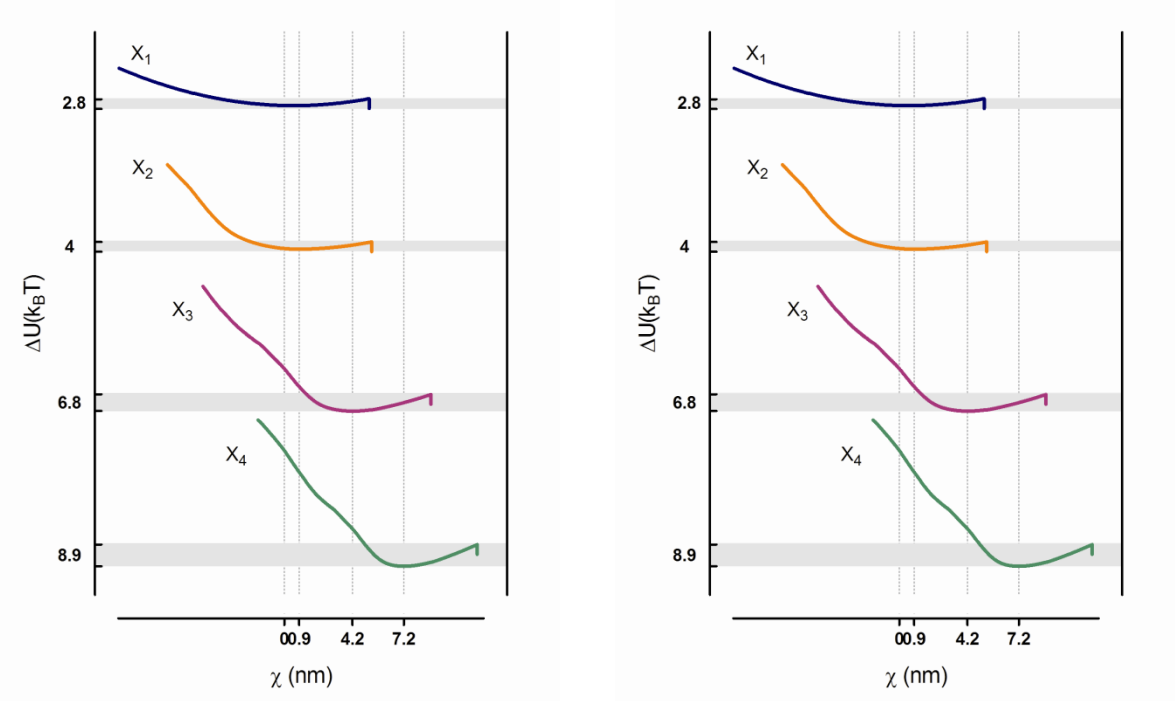

Figure 3.5 Energy landscapes for the prototypical design with a backbone flexural rigidity of 2 pN/nm, states X_1 to X_4 (left) and states X_8 to X_{11} (right)

3.5 Conclusions

The models developed in this chapter address the first mode landscape under the assumptions of a quasi-static equilibrium. These models do not describe the reaction kinetics of receptors and ligands during complex formation. Currently, without sophisticated computational models, this endeavor is one that is more readily investigated through experimentation. If there are known reaction rate constants for the coupled receptor-ligand and receptor-ligand-receptor complex then algorithms such as those developed by Gillespie can be employed.[42,43] However, because of the complex nature of the reaction dynamics, these constants must be determined experimentally and are the subject of future work. In Chapter 4 this is briefly discussed in the context of results.

In this chapter, physical models and simulations of a given Brownian ratchet design were explored. The relationship between landscape energy, elastic properties of the backbone and complex and force-bond energy relationships was discussed. In the next chapter, self-assembled DNA based devices are presented.

Chapter 4

Building and Testing Self-Assembled Ratchets using DNA Origami

In this chapter, the creation, characterization and testing of second generation devices is addressed. These devices were fabricated using self-assembled DNA/hapten motifs. My motive for producing these devices was to gain a more precise understanding of the ratcheting dynamics, design constraints and as a whole to provide more compelling evidence that design with Brownian ratcheting is feasible. The creation of self-assembled devices using these methods allowed for the precise positioning of receptor molecules as well as control of the strain energy landscape for both the receptor complex and the backbone. Self-assembly also allowed the production of devices in biologically relevant quantities. This feature alleviates experimental hurdles in analyzing and testing potential technological adaptations.

4.1 DNA self-assembly

DNA origami is an emergent technique that allows for the construction of complex nanoscale objects from closely packed bundles of B-form DNA. The technique relies on the programmed arrangement of Watson-Crick base pairs. In DNA origami, structures are assembled from sets of staple and scaffold strands, which are annealed in a one-pot reaction. Annealing takes place over long thermal gradients. The long gradients aid in obtaining the lowest thermodynamic configuration. Numerous forms of DNA origami have emerged over the past two decades as an offspring of the conceptualization of Seaman in 1982.[44] More recent techniques have produced elaborate three dimensional structures facilitated by open source software packages.

4.1.1 2-D DNA Origami

The 2-D origami technique pioneered by Rothemund was the first to enable versatile shape programmability.[45] Through a five step design sequence he provided a methodology to produce 2-D shapes with a spatial resolution of about 6nm. Typical shapes produced using these methods were as large as 100 nm. In addition, he demonstrated larger motifs could be created as assemblies of smaller structures. Details of the design methodology can be found in the literature. A simplified schematic representation is shown in Figure 4.1. This work certainly inspired the more sophisticated techniques in 3-D DNA origami.

4.1.2 3-D Honeycomb Framework

The honeycomb array framework represents the state of the art in 3-D DNA self-assembly and was the primary method employed in my research to construct devices.[46] I adopted this method with small modifications to facilitate the inclusion of receptor molecules. For this reason it is important to discuss in detail.

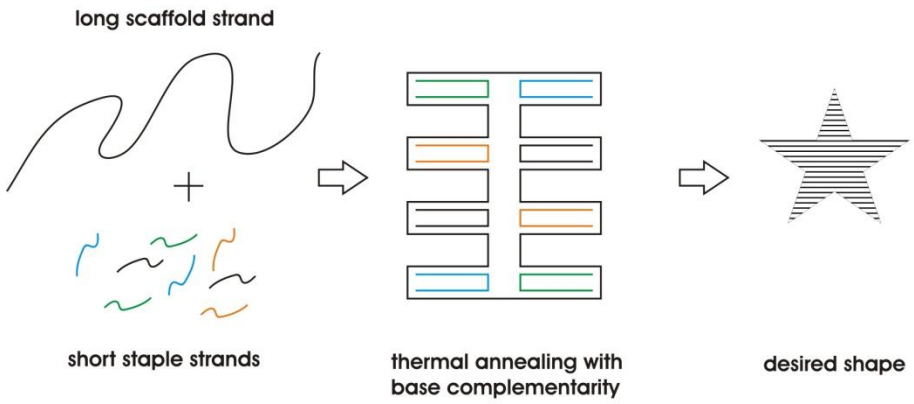

Figure 4.1 Technique pioneered by Rothemund to produce arbitrary 2-D DNA shapes

The honeycomb array framework for assembling DNA places a double helix next to three neighbor helices which forms an octet as shown in Figure 4.2 (left). These helices are connected through anti-parallel cross-over strands. These connections between strands are identical to naturally occurring Holiday Junctions. For B-form DNA the twist density is 10.5 bp per 360º, resulting in possible cross-overs at 240º (7 bp) and 480º (14 bp) and 720º (21 bp) as shown in Figure 4.2 (center and right). Here the crossovers are shown as double lines. Combined octets of

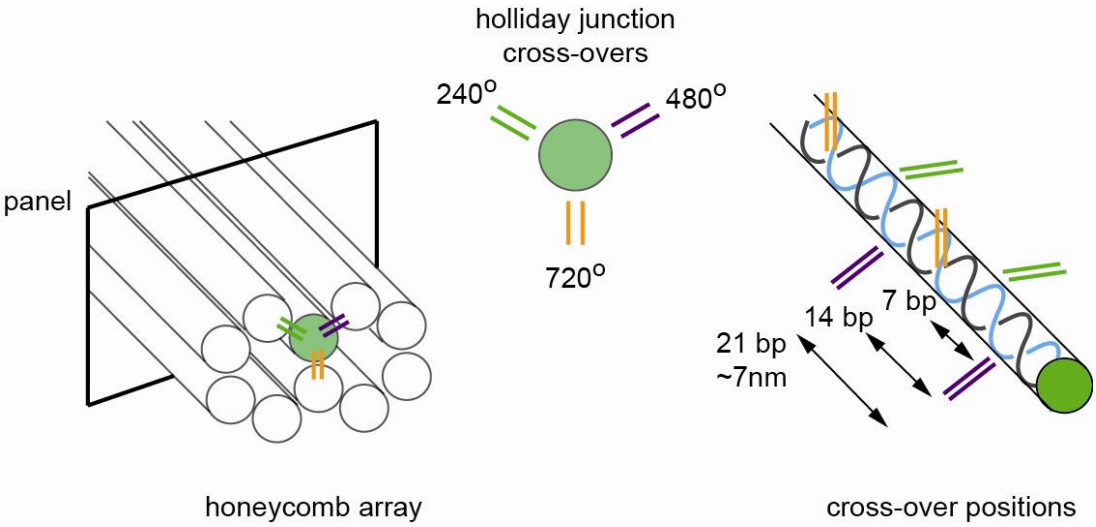

Figure 4.2 Honeycomb array technique pioneered by the Shih Research Group to produce 3-D DNA origami structures.

DNA form a honeycomb structure (panel cross-section in Figure 4.2). Using this method a wide range of 3-D shapes can be created. Numerous shapes have been demonstrated including crosses, beach balls and genie bottles.[45] The honeycomb array framework was recently improved upon to incorporate twists and curves. Using a series of base pair insertions and deletions it was shown

that twists of either handedness could be generated. In addition, stress gradients could be generated that resulted in shape bending with radii as small as 6 nm. This is possible because the physical constraints exerted on a strand by its neighbors leads to the generation of torque orthogonal to the helical axis and bending. In Figure 4.3 an example of an insertion and deletion set used to create bending (left) and twisting (right) is shown. In this figure the insertions and deletions are marked as green and purple bands respectively.

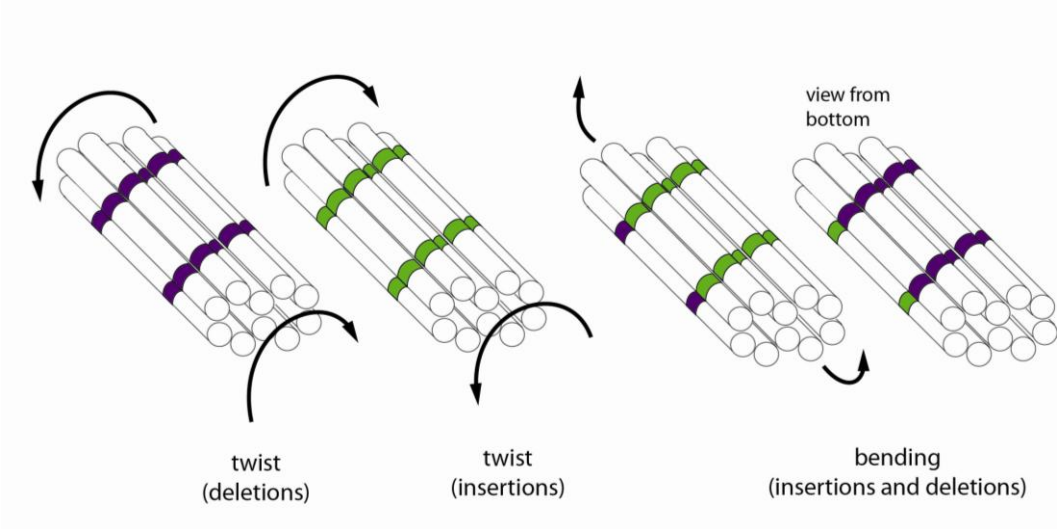

Figure 4.3 Generating bending and twisting using base pair insertions and deletions in honeycomb array DNA origami

4.1.3 Programming Spatial Positioning of Molecules

DNA origami allows for the templating of molecules with nanometer scale resolution. This is often performed by pre-conjugating a label through modification to the 5' phosphate or 3' hydroxyl group on a staple with a known position on the structure. Pre-conjugated strands can often be purchased from suppliers. Conjugation techniques for specific nucleotides exists as well but are less commonly used in this context. Well established techniques involve the use of diamin or Bis-hydrazide and sulfhydryl modifications. An organized list of additional modifications and specific protocols can be found in the literature.[47,48] Several examples of programmed spatial positioning have been shown, including work by Bui et al. where they demonstrated quantum dots could be programmed with 71, 43, 29 and 14 nm periodicities on self assembled nanotubes.[49] This method used a biotin-streptavidan-quantum dot conjugation. The literature offers multitudes of examples for both 2-D and 3-D arrangements.[50-52]

4.2 Brownian Ratchet Design Methodology

My primary goal was to ensure that the observed shape change was indeed a result of the ratchet phenomena. The important distinction between simple shape change and ratcheting is that

ratcheting possesses the ability to generate an aggregate directed force significantly greater than that supplied by the random thermal input (e.g. k_BT). The forces generated through ratcheting can thus be used to perform work. In order to provide evidence of the ratchet phenomena I designed controls that present an energy barrier insurmountable by several k_BT units and designed the active devices such that each barrier (e.g. required barrier between bonding locations) was within the realm of the supplied thermal energy. This ensured ratcheting would take place in the active devices, while the elimination of several ratchets steps (e.g. receptor bonds) in the controls would ensure it did not. Figure 4.4 depicts our ratchet design process.

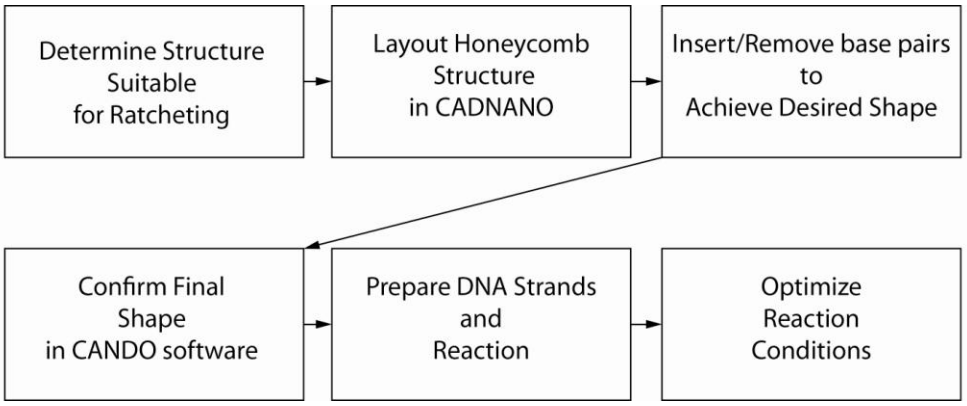

Figure 4.4 Process summary for the creation of honeycomb replete DNA origami structure

4.3 Fabrication of Brownian Ratchet Structures

The fabrication of DNA structures was conducted as described in section 4.2.1 above. Modifications were made to this methodology to incorporate toehold strands containing the receptor molecules for binding. For experimental purposes we chose to use to use a biotin as the receptor and streptavidin as the ligand. The tetravalent nature of streptavidin ensures that sandwich bonding was likely (e.g multiple epitopes). The sequences for the scaffold and staple strands along with the layout are provided in the Supplement, section B.2. Examples of fabricated structures are shown in Figure 4.5.

4.3.1 Reaction Conditions

Device reactions were performed in a 100 ul one-pot reaction consisting of 20 nM scaffold strands and 120 nM of each staple stand in a buffer containing 5 mM Tris, 1 mM ETDA and 18 mM $MgCl_2$. In preliminary studies I assessed the optimal $MgCl_2$ concentration over a sequence of concentrations ranging from 12 mM $MgCl_2$ to 26 mM $MgCl_2$. Staple strands were purchased from Sigma Aldrich normalized to 10 nmoles. The receptor staples strands were purchase from IDT with a 5' modified single biotin (the receptor). We used the viral plasmid, mp13mh18 (New England Biosciences), for the scaffold strand. This a single strand plasmid consisted of 7249 bp.

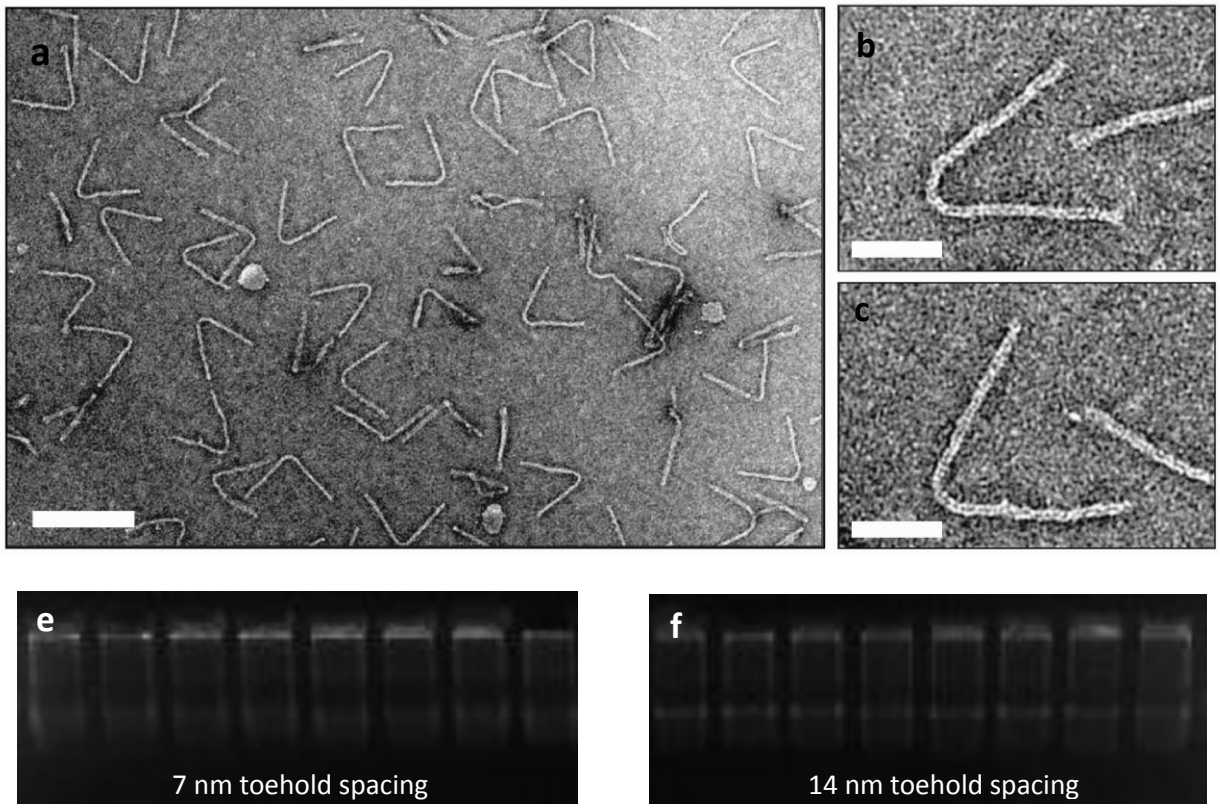

Figure 4.5 Self-assembled DNA structures (left) Electron tomography of devices. (right) close up of devices at two characteristics angles (top) a large number of devices assembled with interior angles of approximately ~40 degrees (bottom) resultant devices also appeared with interior angles of ~80 degrees. Electrophoresis images of self-assembled devices. Devices with toeholds spaced at 7nm and 14 nm formed over a range of $MgCl_2$ concentrations from 12 mM to 26 mM. These are shown as references.

The reaction was thermally annealed over a three step gradient with times ranging from 126 hrs to 168 hrs. An initial melt of the DNA was performed for 2 minutes at 80 ºC. Subsequently, a pre anneal was performed with a thermal ramp from 80 ºC to 60 ºC over a period of 2 hrs. The reaction was then subjected to a long anneal from 60 ºC to 24 ºC over a time period ranging between 124 hrs to 166 hrs. We observed minor increases for the yield at times greater than 124 hrs. Short annealing times (< 60 hrs) produced immeasurable quantities of devices.

4.3.2 Device Purification

Properly formed devices were purified in a two step processes using gel purification and gel extraction. The large molecular weight and size of the device (~4,500,000 daltons, variable with toehold configuration) required the use of agarose gels with median pore sizes approximating the size of the device. Larger pore sizes caused poorly formed bands which ultimately resulted in an inability to obtain high concentrations. Correlations between agarose pore size and percent weight agarose have been characterized using AFM. Aliquots from the reaction were first mixed with 3:1 solution containing loading buffer (Blue Juice 10x, New England Biosciences) and run on 1.75 % agarose gels made in a solution of 11 mM $MgCl_2$. Gels were run on horizontal and vertical gel electrophoresis setups.

The horizontal gels provided better band resolution and higher fidelity purification while vertical gels allowed higher concentrations to be purified. The vertical gels allowed more reacted devices to be simultaneously loaded and subsequently condensed them into a smaller gel area. The later method was necessary to concentrate devices in quantities sufficient for streptavidin reaction studies. Vertical gels were run on 1.5 mm gel slabs for approximately 2 hrs in 0.5x TBE containing 11 mM $MgCL_2$. Horizontal gels were run under the same conditions. Figure 4.6c presents various horizontal gel images of devices. The device band is distinguishable and varies slightly in speed with the presence and number of toeholds. Incorrectly formed structures run at slower speeds. In sets containing toeholds the device band is followed by a forward smear that results from toeholds not being present as seen in the figure. In devices without toeholds the device band is the fastest running band and presents no forward smear (not shown).

4.4 Experimental Setup

All reactions of streptavidin with functional devices were performed at 25 ºC. The concentration of purified devices was first measured on a Qubit fluorescent high sensitivity double stranded DNA reader. A desired concentration of streptavidan (variable with experiment) was then prepared in 1x PBS 7.4. The aliquots were then gently combined and placed in the PCR for 40 minutes. Devices were then imaged directly by TEM or run on a gel. The results, design of controls and variables for these reactions are discussed below.

4.4.1 Topology of Active and Control devices

Four device variants were designed and constructed with identical backbone topologies and variable toeholds configurations. The two active device sets possessed 15 nm long toeholds with a functional biotin group. The toehold spacing was varied between 7nm and 14nm. The two control sets had strategically placed receptor molecules, which created a condition such that full closure of the device would not be observed if ratcheting was not primary mechanism driving movement of the device. The toehold layouts for these device sets are shown below (Figure 4.6a). The design of the toehold itself is shown in 4.6 b. In Figure 4.6c gel bands of devices post assembly are shown. The 7 nm device moves slightly slower through the gel as a result of its higher molecular weight and the encumbrance that larger number of dangling toeholds presents.

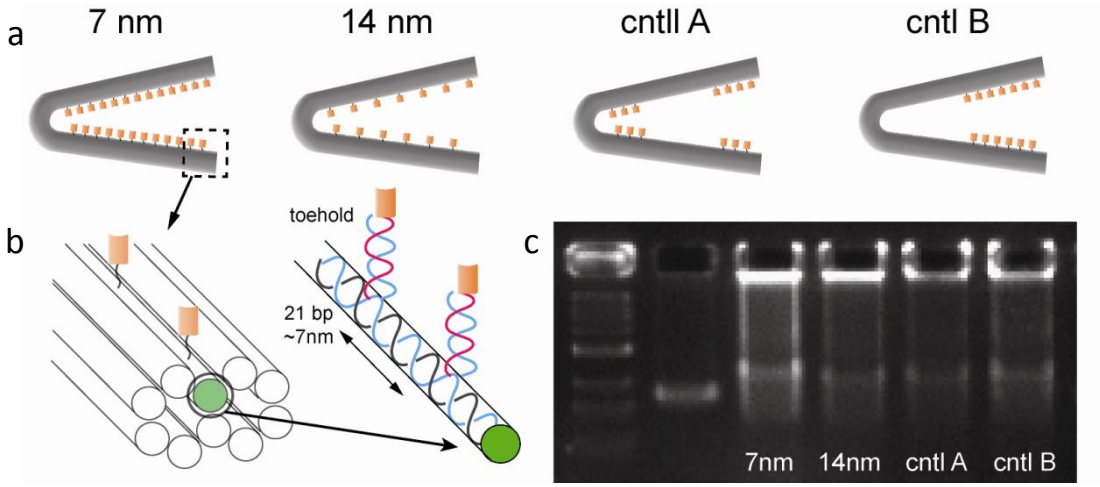

Figure 4.6 Topology of active and control devices. (a) device schema for individual device types (b) device cross-section and toehold configuration (c) gel bands for each device type

4.4.2 Agarose Gel Imaging of Device Response

Agarose gel separation was used to purify devices that self-assembled properly. The yield I observed using the DNA origami the techniques is about 1-2%. For a 100 ul reaction containing 20 nM of scaffold strands, typical resultant concentrations were on the order of 0.2 nM to 0.4 nM after purification. Figure 4.7a shows the reacted gel response. The forward band which appears at approximately 500 bp is the reacted device in the closed conformation. The devices with 14 nm spacing between toeholds showed a less pronounced response as a consequence of the larger energy barrier that must bridged between states. In controls A and B, full closing is not observed. A high contrast image (not shown) indicated that some closing may be present in Control A which is consistent with the first three toeholds forming sandwich bonds and the thermal energy band created by toehold omissions not being surmountable. In control B no closing was observed, despite having a comparable number of toeholds to the device with 14 nm spacings.

4.4.3 Electron Tomography of Device Response

Characterization of the device response was also obtained by TEM. Figure 4.7e through 4.7h shows images of reacted 7nm devices reacted with a 1000:1 streptavidin to device concentration. The streptavidin molecules can be seen down the centerline. The distance between opposing arms the ratchet measures ~20 the approximate high of the dry form DNA sandwich bond. Figure 4.7i shows another artifact we observed at these concentrations – the strep mediated device dimer formation. This artifact can also be seen on the gel image in Figure 4.7a. Here these devices appear as band that moves at about half the speed of a single device. To a lesser degree we also observed trimer formation (faint band at approximately 6k bp). The majority of devices did not react. An un-reacted device is shown in Figure 4.7j. To confirm that particle in the centerline was streptavidin we took a close up image (Figure 4.7j insert).

4.5 Determination of Concentration Dependent Response

In order to explore the relative concentrations of device to streptavidin influenced the response I characterized the response for devices with both 7 nm and 14 nm toeholds spacings My expectation was that at high concentrations no response would be observed as a result of the saturation of the receptors before ratcheting could take place. Studies were performed on a logarithmic concentration ratio curve ranging from 0:1 to 10^6:1 (streptavidin molecules:devices).

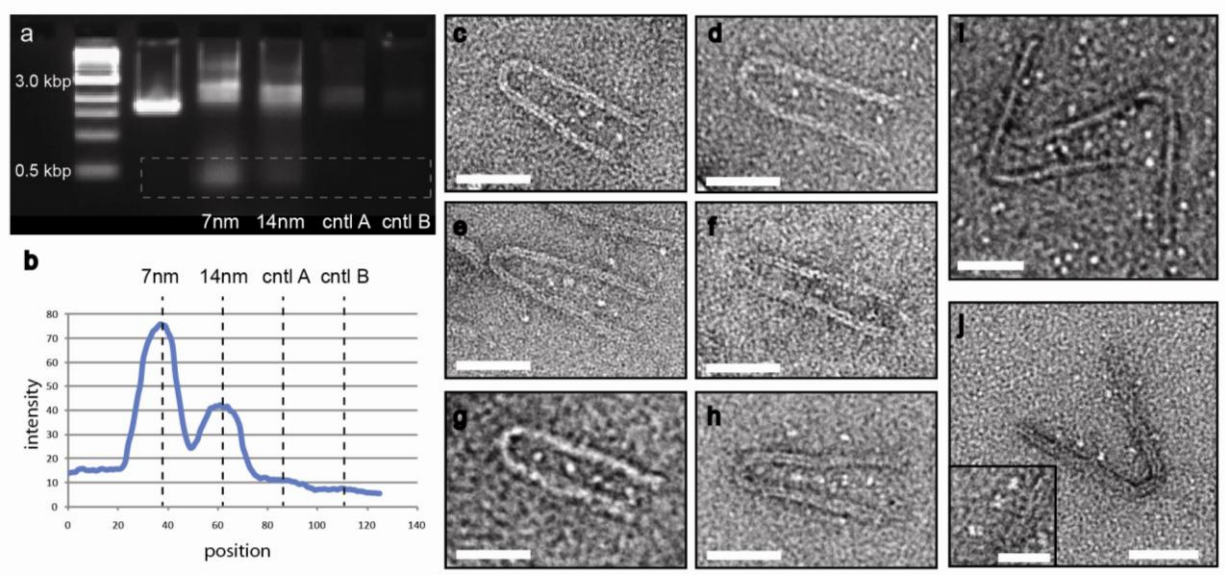

Figure 4.7 Active and control device response, scales are 50 nm, insert scale is 10 nm (a) Gel characterization of response (b) fluorescent intensity of ratcheted band (c) to (h) negative stain TEM images of single ratcheted devices (i) dimer formation (j) device that failed to ratchet, (insert) high magnification TEM confirming bound molecule is tetravalent streptavidin

4.5.1 Agarose Gel Analysis

In Figure 4.8 gel images are presented. These gels present a story and raise questions for future work. Both gels exhibit a similar trend, however, the 14 nm device (Figure 4.7b) produces a less pronounced response. At very low concentration ratios of 10:1 (streptavidin:devices) very few devices have reacted as indicated by the relatively weak fluorescent intensity. In addition, the low concentrations generate more device dimers (band b2) as a result of the absence of free ligand. A pronounced reaction begins to place at about 100:1, where in addition, trimers (band b2) begin forming. The formation of dimers and trimers gradually decreases with increasing concentration. At concentrations of about 1000:1, a new reaction band appears (band b3) and the faster reaction band (band b4) begins fading. We have not characterized the shape of devices in band b3 but speculate, based on their speed in the gel, which they must be in a closed or nearly closed conformation.

By inspecting the aggregate intensity for bands b3 and b4, it is suggestive that the total number of closed remains constant passed a threshold concentration. Rough simulations of the reaction kinetics using Gillespie algorithms[42,43] suggest that these results might occur because of the artificially high concentration of receptors to ligands (at all ligand concentrations) in the nano-environment of the device. These simulations and results will be one of the subjects of future work.

4.6 Discussion

The results presented in this chapter indicate that Brownian ratcheting is indeed taking place. The forces generated by the ratchet were sufficient to bend a double honeycomb DNA structure. Significantly higher forces can be generated by using alternate receptor topologies. In addtion additional characterization was performed to examine the effects of concentration on the ratcheting phenomena for this structure. The specific case of dimer and trimer formation, I believe, can be eliminated through the use of steric hindrances built into the shape.

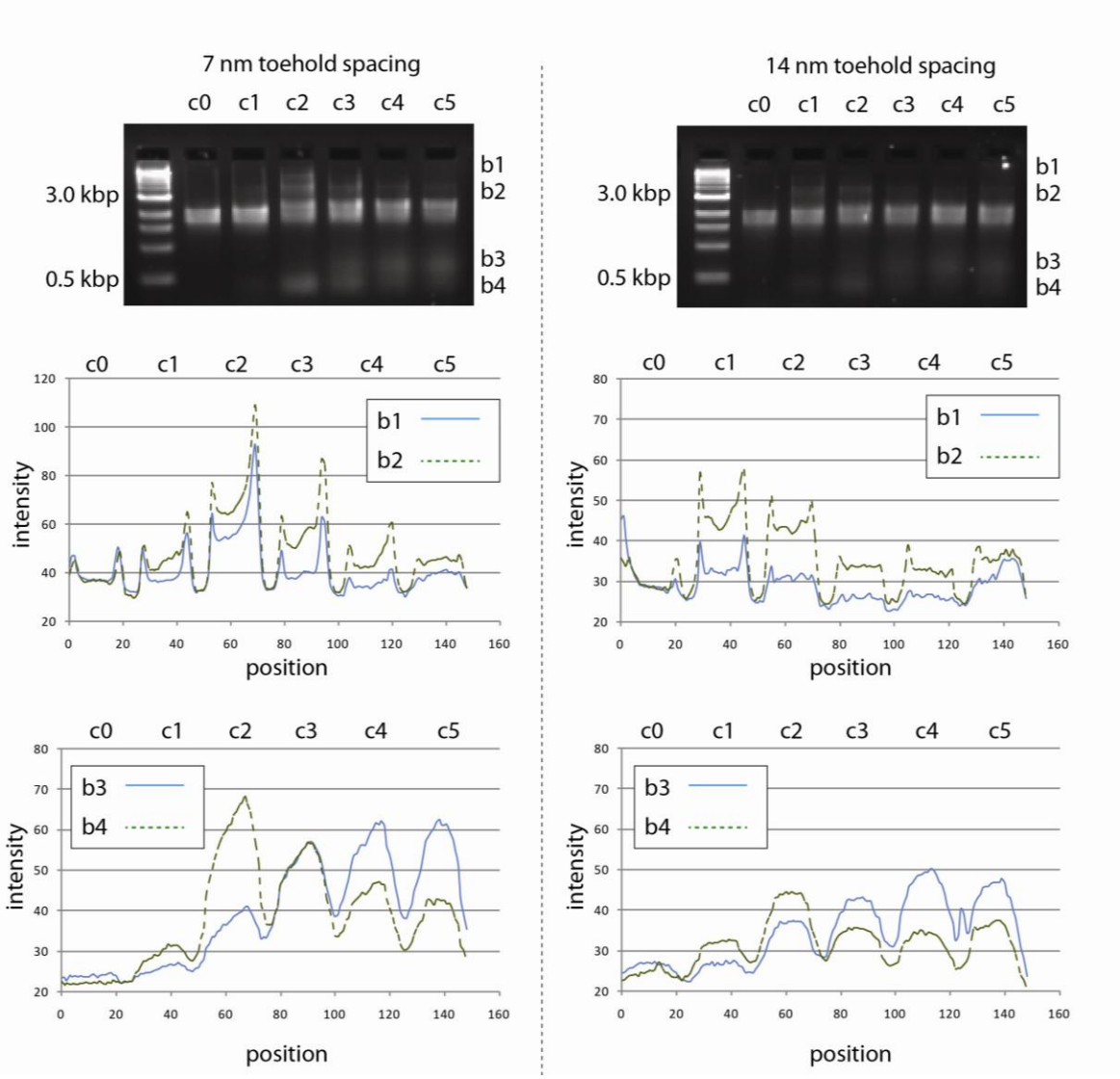

Figure 4.8 Agarose Gel of Reacted Devices at various concentrations (left) 7 nm devices, relative concentration ratio varies from 0 to 10^6:1 (right) 14 nm devices, relative concentration ratio varies from 0 to 10^6:1

Bibliography

(1) Keller, D.; Bustamante, C. *Biophysical Journal* **2000**, *78*, 541-556.

(2) Mahadevan, L. *Science* **2008**, *95*.

(3) Hänggi, P. *Reviews of Modern Physics* **2009**, *81*, 387-442.

(4) Mahadevan, L. *Science* **2000**, *288*, 95-99.

(5) Peskin, C. S. Odell, G. M.; Oster, G. F. *Biophysical journal* **1993**, *65*, 316-24.

(6) Cruz, S.; Biology, C. **2002**, *323*, 315-323.

(7) Magnasco, M. O. Forced thermal ratchets. *Physical Review Letters* **1993**, *71*, 1477-1481.

(8) Fiasconaro, a; Ebeling, W.; Gudowska-Nowak, E. *The European Physical Journal B* **2008**, *65*, 403-414.

(9) Tilney, L. G.; Portnoy, D. a *The Journal of cell biology* **1989**, *109*, 1597-608.

(10) Astumian, R. D. *Science* **2009**, *917*.

(11) Astumian, R. D. *Science* **1997**, *276*, 917-922.

(12) Janmey, P. a; McCulloch, C. a *Annual review of biomedical engineering* **2007**, *9*, 1-34.

(13) Features, D. Microtubules, O. F.; Dark-field, B. Y. *Development* **1990**, *26*, 135-156.

(14) Theriot, J. a; Mitchison, T. J. Tilney, L. G.; Portnoy, D. a The rate of actin-based motility of intracellular Listeria monocytogenes equals the rate of actin polymerization. *Nature* **1992**, *357*, 257-60.

(15) Wang, H. *Journal of physics. Condensed matter : an Institute of Physics journal* **2005**, *17*, S3997-4014.

(16) Detailed Balance Symetry 1931.pdf.

(17) Kay, E. R. Leigh, D. A.; Zerbetto, F. *Molecular Devices Synthetic Molecular Motors and Mechanical Machines Angewandte*; 2007; pp. 72 - 191.

(18) Evans, E.; Ritchie, K. *Biophysical journal* **1997**, *72*, 1541-55.

(19) Bustamante, C. Chemla, Y. R. Forde, N. R.; Izhaky, D. *Annual review of biochemistry* **2004**, *73*, 705-48.

(20) Chon, J. W. M. Mulvaney, P.; Sader, J. E. *Journal of Applied Physics* **2000**, *87*, 3978.

(21) Sader, J. E. *Journal of Applied Physics* **1998**, *84*, 64.

(22) Tinoco, I.; Bustamante, C. *Biophysical chemistry* **2002**, *101-102*, 513-33.

(23) Saphire, E. O. Stanfield, R. L. Crispin, M. D. M. Parren, P. W. H. I. Rudd, P. M. Dwek, R. a; Burton, D. R.; Wilson, I. a *Journal of molecular biology* **2002**, *319*, 9-18.

(24) Hirlekarschmid, a; Stanca, S. Thakur, M. Thampi, K.; Ramansuri, C. *Sensors and Actuators B: Chemical* **2006**, *113*, 297-303.

(25) Lomant, a J.; Fairbanks, G. *Journal of molecular biology* **1976**, *104*, 243-61.

(26) Danczyk, R. Krieder, B. North, a; Webster, T. HogenEsch, H.; Rundell, a *Biotechnology and bioengineering* **2003**, *84*, 215-23.

(27) Vikholm, I.; Albers, W. M. *Langmuir* **1998**, *14*, 3865-3872.

(28) Bonroy, K. Frederix, F. Reekmans, G. Dewolf, E. De Palma, R. Borghs, G. Declerck, P.; Goddeeris, B. *Journal of immunological methods* **2006**, *312*, 167-81.

(29) Hermann, R. Walther, P.; Müller, M. *Histochemistry and cell biology* **1996**, *106*, 31-9.

(30) Heussinger, C. Bathe, M.; Frey, E. **2008**, *1*, 1-4.

(31) Measurements, F.-extension *Biophysical Journal* **1999**, *76*, 409-413.

(32) Grubmüller, H. *Methods in molecular biology (Clifton, N.J.)* **2005**, *305*, 493-515.

(33) Hanasaki, I. Haga, T.; Kawano, S. *Engineering* **2008**, *255238*.

(34) Heymann, B.; Grubmüller, H. *Chemical Physics Letters* **1999**, *303*, 1-9.

(35) Hanasaki, I. Haga, T.; Kawano, S. *Journal of Physics: Condensed Matter* **2008**, *20*, 255238.

(36) Schwesinger, F. Ros, R. Strunz, T. Anselmetti, D. Güntherodt, H. J. Honegger, a; Jermutus, L. Tiefenauer, L.; Pluckthun, a *Proceedings of the National Academy of Sciences of the United States of America* **2000**, *97*, 9972-7.

(37) Heymann, B.; Grubmuller, H. *Chemical Physics Letters* **1999**, 425-432.

(38) Oesterhelt, F. Rief, M.; Gaub, H. E. *New Journal of Physics* **1999**, *1*, 1-11.

(39) Berquand, A. Xia, N. Castner, D. G. Clare, B. H. Abbott, N. L. Dupres, V. Adriaensen, Y.; Dufrêne, Y. F. *Langmuir : the ACS journal of surfaces and colloids* **2005**, *21*, 5517-23.

(40) Gullingsrud, J. R. Braun, R.; Schulten, K. *Journal of Computational Physics* **1999**, *211*, 190-211.

(41) Douglas, S. M. Dietz, H. Liedl, T. Högberg, B. Graf, F.; Shih, W. M. *Nature* **2009**, *459*, 414-8.

(42) Gillesple, D. T. **1977**, *93555*, 2340-2361.

(43) Hayot, F.; Jayaprakash, C. *Population (English Edition)* **2006**, 1-19.

(44) Lee, J. B. Roh, Y. H. Um, S. H. Funabashi, H. Cheng, W. Cha, J. J. Kiatwuthinon, P. Muller, D. A.; Luo, D. *Nature Nanotechnology* **2009**, *4*.

(45) Rothemund, P. W. K. *Nature* **2006**, *440*, 297-302.

(46) Dietz, H. Douglas, S. M.; Shih, W. M. *Science (New York, N.Y.)* **2009**, *325*, 725-30.

(47) Leclere, P. Surin, M. Brocorens, P. Cavallini, M. Biscarini, F.; Lazzaroni, R. *Materials Science and Engineering: R: Reports* **2006**, *55*, 1-56.

(48) The, I. *Methods* **1994**, *34*.

(49) Bui, H. Onodera, C. Kidwell, C. Tan, Y. Graugnard, E. Kuang, W. Lee, J. Knowlton, W. B. Yurke, B.; Hughes, W. L. *Nano letters* **2010**, *10*, 3367-72.

(50) Voigt, N. V. Tørring, T. Rotaru, A. Jacobsen, M. F. Ravnsbæk, J. B. Subramani, R. Mamdouh, W. Kjems, J. Mokhir, A. Besenbacher, F.; Gothelf, K. V. *Nature Nanotechnology* **2010**, *5*, 200-203.

(51) Hillebrenner, H. Buyukserin, F. Stewart, J. D.; Martin, C. R. *Nanomedicine (London, England)* **2006**, *1*, 39-50.

(52) Stephanopoulos, N. Liu, M. Tong, G. J. Li, Z. Liu, Y. Yan, H.; Francis, M. B. *Nano letters* **2010**, *10*, 2714-20.

Appendix A

Supporting Electron Micrographs of Nanowire Response

Active Device, 1 μm (Initial Condition)	Active Device, 1 μm (Response, 1.67 μM Streptavidin)
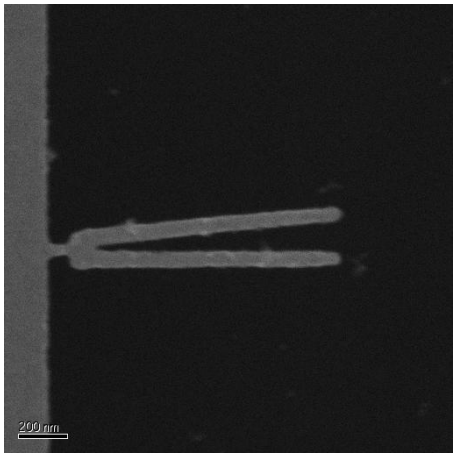	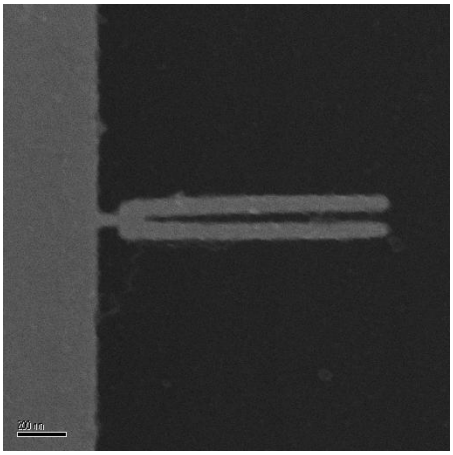
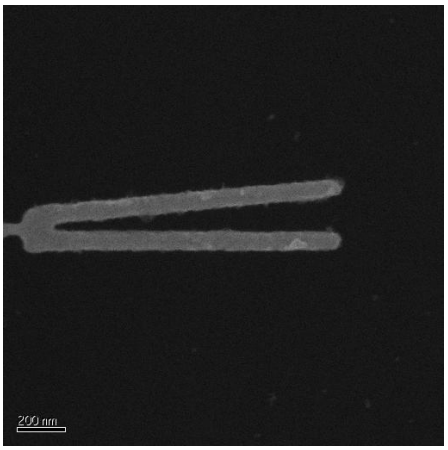	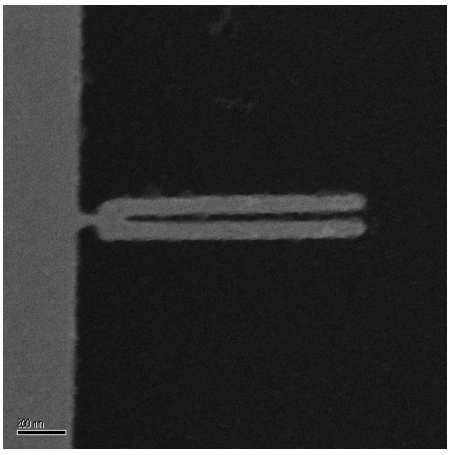
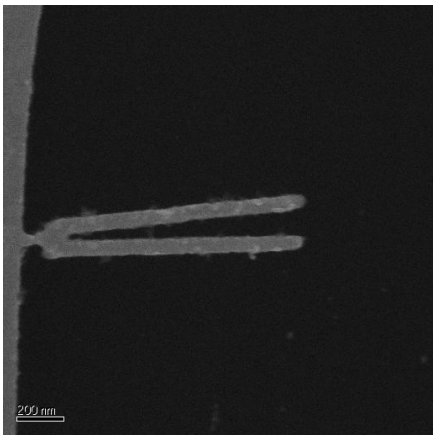	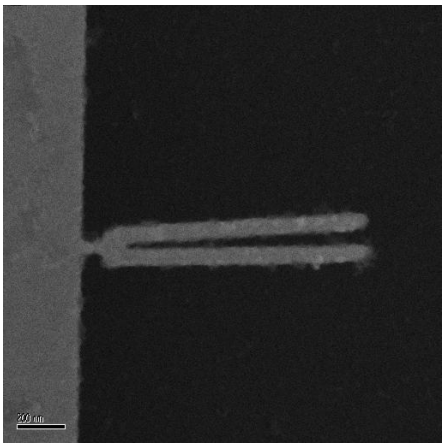

Active Device, 2 μm (Initial Condition)	Active Device, 2 μm (Response, 1.67 μM Streptavidin)
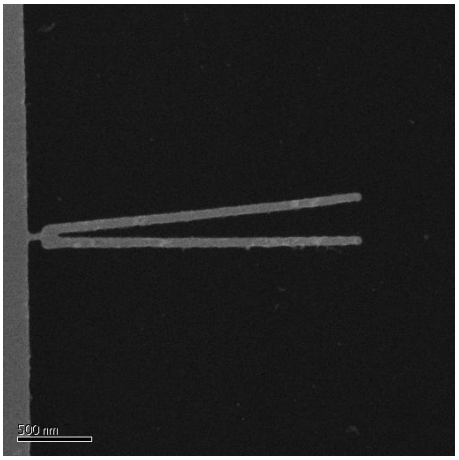	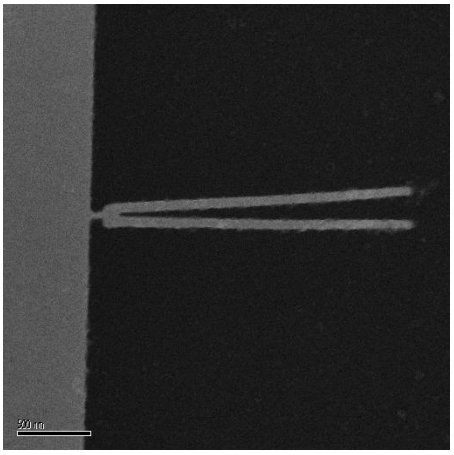
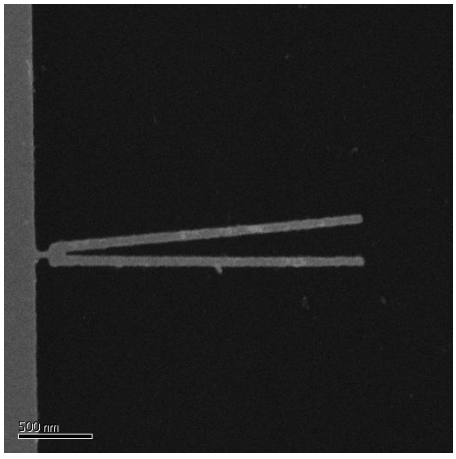	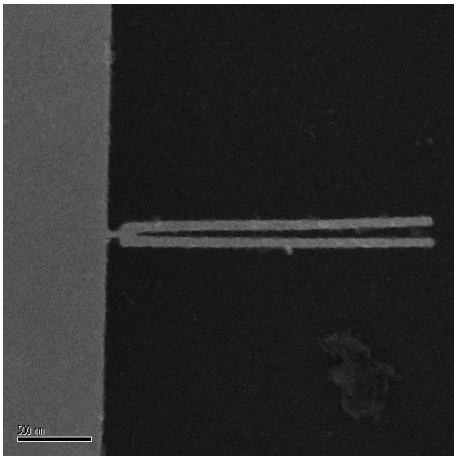
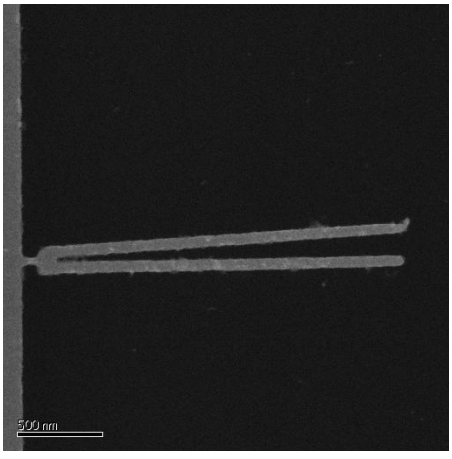	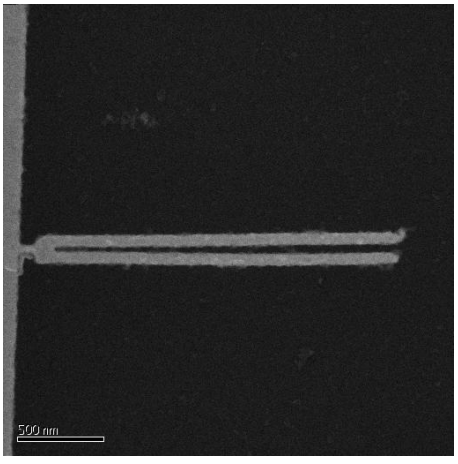

Control Device, 1 μm (Initial Condition)	Control Device, 1 μm (Response, No Streptavidin)
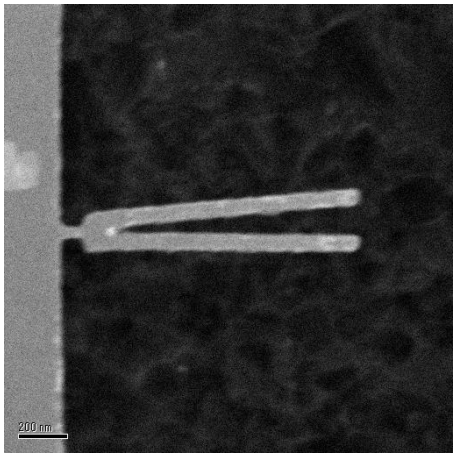 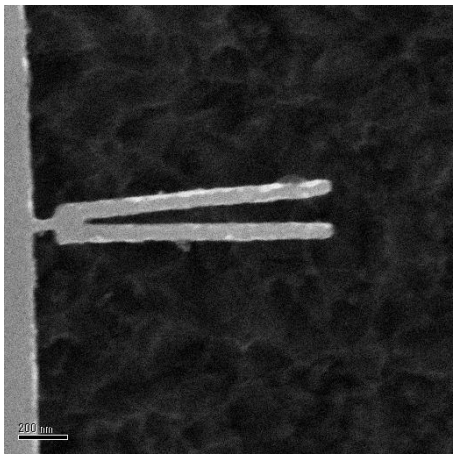 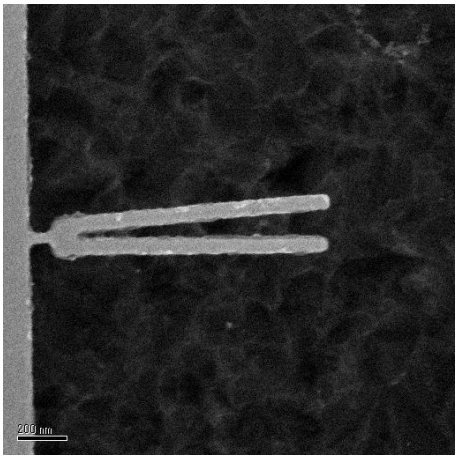	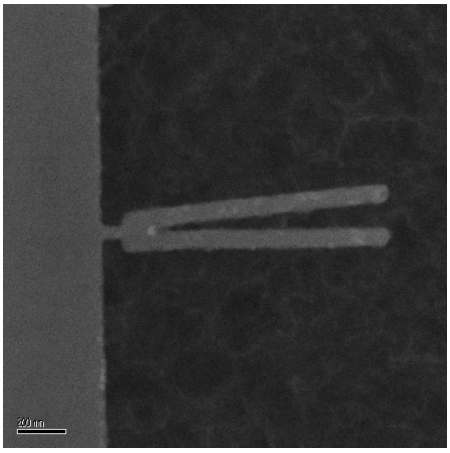 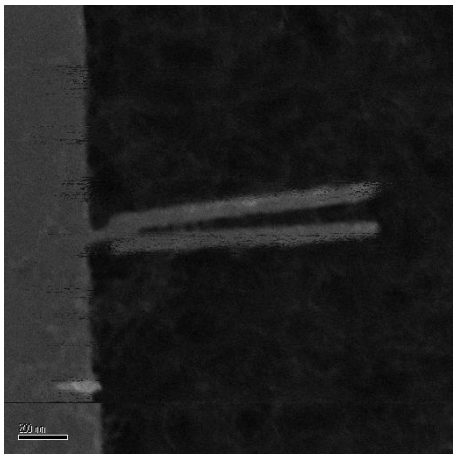 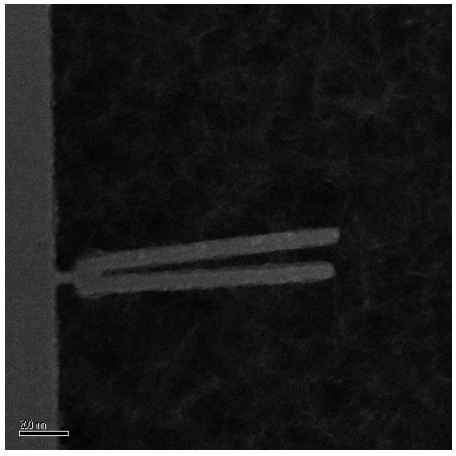

Control Device, 2 μm (Initial Condition)	Control Device, 2 μm (Response, No Streptavidin)
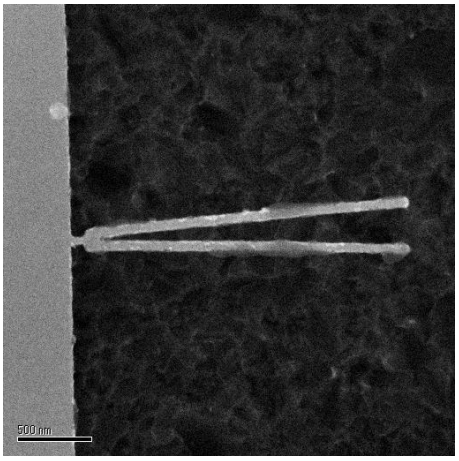	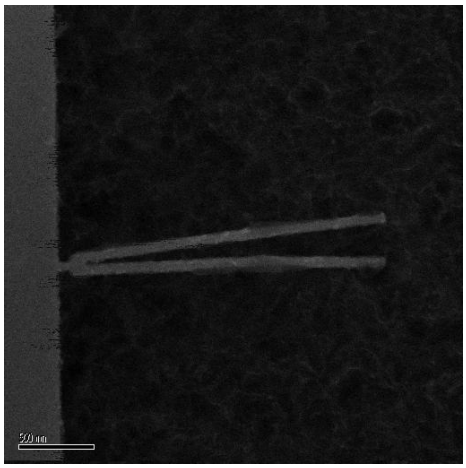
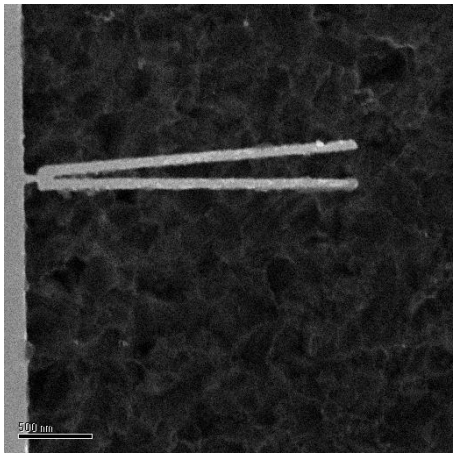	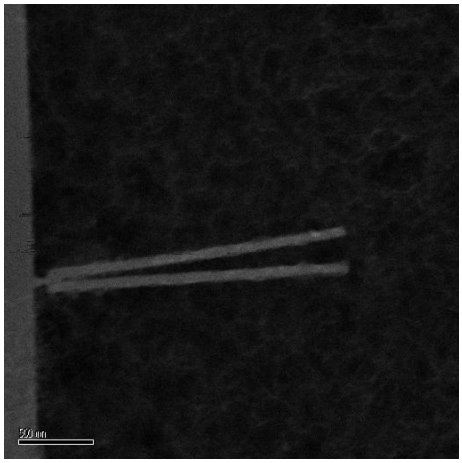
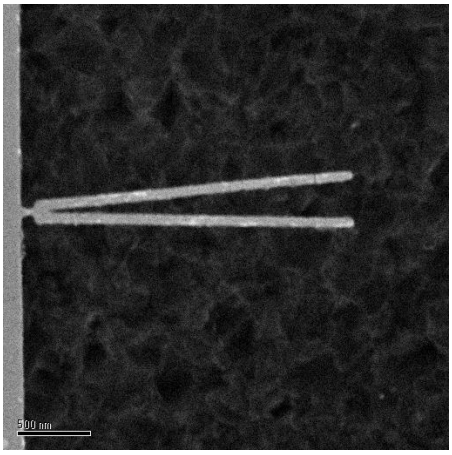	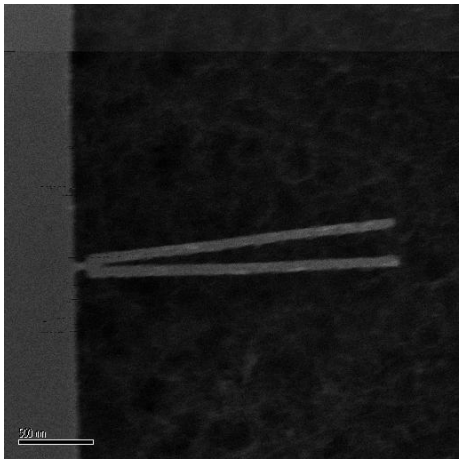

Appendix B

Sader Model of nanowire vibrations in a viscous medium

```
function [temp, A3db,freqccc] = SaderNanowire3()

%%%%%%%%%%%%%%%%%%%%%%%%%%%%%%%%%%%%%%%%%%%%%%%%%%%%%%%%%%%%%%%%%%%%%%%%%%%%%%%
% A. Input descrition and constants
%%%%%%%%%%%%%%%%%%%%%%%%%%%%%%%%%%%%%%%%%%%%%%%%%%%%%%%%%%%%%%%%%%%%%%%%%%%%%%%

%L = length of beam in m
%D = diameter of beam in m
%E = GPa->N/m^2 Young's Modulus
%mat = material number (0 -> gold, 1 -> dna)


C1 = 1.875104; %smallest positive root of 1+cos(Cn)*cosh(Cn) = 0
density_water = 997.0794; %kg/m^3   1000=water, 1.18=air
visc_water = 8.5692e-4; %Ns/m^2   1.002e-3 = water, 1.77e-5 = air
Temp=300;
kb = 1.3806505e-23;  % J/K boltzmann
nmax = 6; %originally set to six by babak I changed trying to figure out the
meaning

kbt = kb*Temp;
%%%%%%%%%%%%%%%%%%%%%%%%%%%%%%%%%%%%%%%%%%%%%%%%%%%%%%%%%%%%%%%%%%%%%%%%%%%%%%%
% B. Input descrition and constants
%%%%%%%%%%%%%%%%%%%%%%%%%%%%%%%%%%%%%%%%%%%%%%%%%%%%%%%%%%%%%%%%%%%%%%%%%%%%%%%
L=125e-9;
D=20e-9;
thick = 20e-9;
mat=1;
rect=1;
air=0;
plotall=0;

if mat == 0 %gold
    E = 78E9;% manufacturer
    density = 19300; %19.3 g/cm^3 19.3/1000*100*100
end

if mat == 1 %dna
    E = .1e9;
    density = 1380;
end

if air == 1 %in air, not water
    density_water = 1.1778; %kg/m^3   1000=water, 1.18=air
    visc_water = 1.8527e-5; %Ns/m^2   1.002e-3 = water, 1.77e-5 = air
end

if rect == 1 %is it a rectangle
```

```
    I = D*thick^3/12;
    mu = density*D*thick;
else
    I=pi/64*D^4; %Area moment of inertia (2nd moment)
    mu = density*pi*(D/2)^2; % mass/length
end

%%%%%%%%%%%%%%%%%%%%%%%%%%%%%%%%%%%%%%%%%%%%%%%%%%%%%%%%%%%%%%%%%%%%%%%%%%%%%%%
% C. Sadar model
%%%%%%%%%%%%%%%%%%%%%%%%%%%%%%%%%%%%%%%%%%%%%%%%%%%%%%%%%%%%%%%%%%%%%%%%%%%%%%%

%find C values
%near = [1.8 5 8 11.2 14.2
nearx = 1.8;
C = [];
ncount = 0;
while ncount < nmax
    val = fzero('1+cos(x)*cosh(x)',nearx);
    nearx = nearx+1;
    if isempty(find(abs(C-val)<0.00001))
        C = [C val];
        ncount = ncount+1;
    end
end


%get some constants
w_vac = C(1)^2/L^2*sqrt(E*I/mu); %fundamental
f=w_vac/(2*pi) %resonant frequency in a vacuum
k=3*E*I/L^3 %stiffness

%in water, the traditional way
f_fluid = f * (1+pi*density/4/density_water)^(-0.5);
w_fluid = f_fluid*2*pi;

delta=0.0005;
w=w_vac*(0.001:delta:8);
mo = mu*L;
dfdm = 0.279*sqrt(E*I/L^3/mo^3);

%now using hydrodynamic function
syms x;
Re=density_water*w*D^2/4/visc_water; %Reynolds, w vs w_vac?1
T=1+(4*i*besselk(1, -i*sqrt(i*Re)))./(sqrt(i*Re).*besselk(0, -i*sqrt(i*Re)));

if rect == 1 %rectangle correction
   tau = log10(Re);
   omega_real = (.91324-.48274.*tau+.46842.*tau.^2-
.12886.*tau.^3+.044055.*tau.^4)./(1-.56964.*tau+.4869.*tau.^2-
.13444.*tau.^3+.045155.*tau.^4);
   omega_imag = (-.024134-.029256.*tau+.016294.*tau.^2-
.00010961.*tau.^3+.000064577.*tau.^4)./(1-.59702.*tau+.55182.*tau.^2-
.18357.*tau.^3+.079156.*tau.^4);
   T = T.*(omega_real + i*omega_imag);
```

```
end

B = C(1)*sqrt(w/w_vac).*(1+pi*density_water*D^2/4/mu*(T)).^(1/4);
phi = (cos(C.*x)-cosh(C.*x)) +
(cos(C)+cosh(C))/(sin(C)+sinh(C)).*(sinh(C.*x)-sin(C.*x));

x=1;
for n = 1:nmax, %each mode
    alpha(n,:) = 2*sin(C(n)).*tan(C(n)) ./ (C(n).*(C(n).^4-
B.^4).*(sin(C(n))+sinh(C(n))));
    intsum(n) = trapz(w, (abs(alpha(n,:)).^2));
    W2sum(n,:)= 3*pi*kb*Temp/k * (abs(alpha(n,:)).^2) ./ (C(n).^4 .*
intsum(n))*eval(phi(n)).^2;
end

top = sqrt(max(sum(W2sum, 1)));
DC = sqrt(sum(W2sum,1));
DC = DC(1);
ind = find(sqrt(sum(W2sum,1))<DC/2, 1, 'first');
tdb = w(ind)/2/pi;

%%%%%%%%%%%%%%%%%%%%%%%%%%%%%%%%%%%%%%%%%%%%%%%%%%%%%%%%%%%%%%%%%%%%%%%%%%%%
% D. Amplitude response probabilities
%%%%%%%%%%%%%%%%%%%%%%%%%%%%%%%%%%%%%%%%%%%%%%%%%%%%%%%%%%%%%%%%%%%%%%%%%%%%
%find the corner freequency (check this logic)
A3db = top/(exp(3/20));
temp = sqrt(real(sum(W2sum(1:nmax,:),1)));
freqccc = w/(2*pi);
i_corner = interp1(temp,freqccc,A3db);
BW = i_corner;

%determine the variance of the displacement
dhzoutsquared = real(sum(W2sum(1:nmax,:),1));
f_gabe=w/2/pi;
integ1 = cumtrapz(f_gabe,dhzoutsquared);
sigma_g = sqrt(integ1(end));

%equipartition at 1kbt (average energy transferred, used as know reference)
x_equip = sqrt(kbt/k);

%correlate displacement to energy
energy_g = [0:0.1:8]; %in units of kbt
disp = sqrt((kbt*energy_g)./k);

%determine the probability of a given displacement being exceeded
drange = disp;
term1 = (1/(sigma_g*sqrt(2*pi)));
term2 = exp(-(drange.^2/(2*sigma_g^2)));
p1 = term1*term2;

lplot = length(drange)-1;
for n = 1:lplot
aaa = drange(n:end);
bbb = p1(n:end);
```

```
p2 = cumtrapz(aaa,bbb);
p2_x(n) = p2(end);
end

%%%%%%%%%%%%%%%%%%%%%%%%%%%%%%%%%%%%%%%%%%%%%%%%%%%%%%%%%%%%%%%%%%%%%%%%%%%%
% E. False Alarm Rate (i.e the number of crossings or opportunities)
%%%%%%%%%%%%%%%%%%%%%%%%%%%%%%%%%%%%%%%%%%%%%%%%%%%%%%%%%%%%%%%%%%%%%%%%%%%%

Tfa = 1/BW*exp(drange.^2/(2*sigma_g.^2));
Eout = [energy_g; 1./Tfa]';

%%%%%%%%%%%%%%%%%%%%%%%%%%%%%%%%%%%%%%%%%%%%%%%%%%%%%%%%%%%%%%%%%%%%%%%%%%%%
% F. Plots
%%%%%%%%%%%%%%%%%%%%%%%%%%%%%%%%%%%%%%%%%%%%%%%%%%%%%%%%%%%%%%%%%%%%%%%%%%%%

if plotall == 1

figure
colors = 'rgbcmky';
loglog(w/(2*pi),sqrt(real(sum(W2sum(1:nmax,:),1))), 'r--', 'LineWidth',
2);hold on
loglog([i_corner i_corner],[max(temp) min(temp)]); hold off
xlabel('Frequency (Hz)');
ylabel('Thermal noise (m/sqrt(Hz))');

figure
subplot(2,1,1);semilogy(energy_g(1:lplot),p2_x(1:lplot))
subplot(2,1,2);semilogy(drange(1:lplot),p2_x(1:lplot))

figure
semilogy(energy_g,1./Tfa);hold on
xlabel('coupled energy(kBT)')
ylabel('# opportunities/second')

end
```

Appendix C

Matlab Models used in conjunction with parametric FEA in COMSOL.

```
function [ Foutput ] = molecular_forces1(X, Y, u, v, t, hsand, bnd1, x0, G0,
F_unbind,ustrain)

%%%%%%%%%%%%%%%%%%%%%%%%%%%%%%%%%%%%%%%%%%%%%%%%%%%%%%%%%%%%%%%%%%%%%%%%%%%%
% A. Find bonds that have made contact (bonds activated)
%%%%%%%%%%%%%%%%%%%%%%%%%%%%%%%%%%%%%%%%%%%%%%%%%%%%%%%%%%%%%%%%%%%%%%%%%%%%

x = X+u; y = Y+v;
l_coord = sqrt(x.^2 +y.^2);

file_present = exist('state_vector.mat','file')
if file_present ~= 0
    load state_vector.mat
    vl = length(statevv) + 1;
    F_on = zeros(length(x),1);
    index1 = y < hsand/2;
    index2 = (statevv(vl-1).fon == 1);
    F_on(index1) = 1;
    F_on(index2) = 1;
else
    vl = 1;
    F_on = zeros(length(x),1);
    index1 = y < hsand/2;
    F_on(index1) = 1;
end

%%%%%%%%%%%%%%%%%%%%%%%%%%%%%%%%%%%%%%%%%%%%%%%%%%%%%%%%%%%%%%%%%%%%%%%%%%%%
% B. Compute the force and total energy of the sandwich bond
%%%%%%%%%%%%%%%%%%%%%%%%%%%%%%%%%%%%%%%%%%%%%%%%%%%%%%%%%%%%%%%%%%%%%%%%%%%%

stretch = (y-hsand/2);

%Bonds in Compression
index_compression = find(stretch <= 0);
stretch(index_compression) = 0;

%Bonds not turned on (set to zero)
index_off = find(F_on == 0);
stretch(index_off) = 0;

%Force and Energy in Each Molecule
[F_gen, U_PEG, U_out_peg, U_out_bond] =
stretch_landscape_b(stretch,F_unbind);

%Broken Bonds
index_broken = find((F_gen == -1));
```

```
%%%%%%%%%%%%%%%%%%%%%%%%%%%%%%%%%%%%%%%%%%%%%%%%%%%%%%%%%%%%%%%%%%%%%%%%%%%%
% D. Package Output Matrix and Save
%%%%%%%%%%%%%%%%%%%%%%%%%%%%%%%%%%%%%%%%%%%%%%%%%%%%%%%%%%%%%%%%%%%%%%%%%%%%

%Positional Data
statevv(vl).Y = Y;
statevv(vl).X = X;
statevv(vl).x = x;
statevv(vl).y = y;
statevv(vl).l = l_coord;
statevv(vl).t = t;
statevv(vl).stretch = stretch;
statevv(vl).xb = x0-bnd1;

%Bonds in Compression (0=compression)
fcompression = ones(length(x), 1); fcompression(index_compression) = 0;
statevv(vl).fcompression = fcompression;

%Bonds Broken (0=broken)
fbroken = ones(length(x), 1); fbroken(index_broken) = 0;
statevv(vl).fbroken = fbroken.*F_on;

%Bonds Activated (1=activated)
statevv(vl).fon = F_on;

%Output force before on/broken accounted for (bonds in compression removed)
statevv(vl).fgen1 = F_gen;

%Resultant Output Force
Foutput = F_gen.*F_on.*fcompression.*fbroken.*fx;
statevv(vl).fout = Foutput;

%Energy Data
statevv(vl).ubond = sum(F_on.*fbroken.*fx)*G0;
statevv(vl).upeg_all = sum(U_PEG.*fx');
statevv(vl).upeg = U_PEG;
statevv(vl).uout_peg = U_out_peg;
statevv(vl).uout_bond = U_out_bond;
statevv(vl).ustrain = ustrain;
statevv(vl).u = statevv(vl).ubond + statevv(vl).upeg_all...
                + statevv(vl).ustrain;


save('/Users/glavella/Desktop/COMSOL and MATLAB
models/state_vector.mat','statevv')
```

```
function [ ftherm ] = thermal_force( t, xB, bnd1, x0)

%%%%%%%%%%%%%%%%%%%%%%%%%%%%%%%%%%%%%%%%%%%%%%%%%%%%%%%%%%%%%%%%%%%%%%%%%%%%
% This is a force force function, that applies a homogenous force to the
%ratchet to react a given brownian position (xB) then reverse the force
%%%%%%%%%%%%%%%%%%%%%%%%%%%%%%%%%%%%%%%%%%%%%%%%%%%%%%%%%%%%%%%%%%%%%%%%%%%%

file_present = exist('thermal_vector.mat','file');
thermal_unit = 4000e-12;

if file_present ~= 0
    load thermal_vector.mat
    inc = length(v1);

    if (v1(inc).rev == 0)
        ftherm = -5*thermal_unit*t;
        v1(inc+1).rev = 0;
        v1(inc+1).ftherm = ftherm;
        v1(inc+1).t = t;
        v1(inc+1).off = 0;
        if (bnd1 < xB/2)
        v1(inc+1).rev = 1;
        v1(1).t_rev = t;
        v1(1).f_rev = ftherm;
        end

    elseif (v1(inc).rev == 1) && (v1(inc).off == 0)

        ftherm =  v1(1).f_rev + 3*thermal_unit*(t - v1(1).t_rev);
        v1(inc+1).rev = 1; v1(inc+1).ftherm = ftherm;
        v1(inc+1).t = t;

        if bnd1 > x0 + 20e-9
            v1(inc+1).off = 1;
        else
            v1(inc+1).off = 0;
        end

    else
        ftherm = v1(inc).ftherm;% + 1e-20;
        v1(inc+1).rev = 1; v1(inc+1).ftherm = ftherm;
        v1(inc+1).t = t; v1(inc+1).off = 1;
    end

else
    ftherm = -thermal_unit*t;
    v1(1).rev = 0; v1(1).ftherm = ftherm;
    v1(1).t = t; v1(1).off = 0;
end

save('/Users/glavella/Desktop/COMSOL and MATLAB
models/thermal_vector.mat','v1')
end
```

```
function [ F_out, U_out, U_out_peg, U_out_bond ] =
stretch_landscape(elongation, Funbind)

%%%%%%%%%%%%%%%%%%%%%%%%%%%%%%%%%%%%%%%%%%%%%%%%%%%%%%%%%%%%%%%%%%%%%%%%%%%%%%%
%
% Description: Computes the F-D profile and Total Energy of the Stretch
%              PEG Molecule
%
%              Input: vector of stretch molecules [d1...dn] (meters)
%              Ouptut: vector of [F1...Fn] (N) and [U1...Un] (J)
%
%%%%%%%%%%%%%%%%%%%%%%%%%%%%%%%%%%%%%%%%%%%%%%%%%%%%%%%%%%%%%%%%%%%%%%%%%%%%%%%

%%%%%%%%%%%%%%%%%%%%%%%%%%%%%%%%%%%%%%%%%%%%%%%%%%%%%%%%%%%%%%%%%%%%%%%%%%%%%%%
% A. Initial Parameters (obtained from Ref 1)
%%%%%%%%%%%%%%%%%%%%%%%%%%%%%%%%%%%%%%%%%%%%%%%%%%%%%%%%%%%%%%%%%%%%%%%%%%%%%%%
linker = 0; %input 0 indicates PEG molecule in PBS, 1 input polymer (FJC)
            %model

kB = 1.38e-23; T = 300; kBT = kB*T;
L_planar = 0.358e-9; L_helical = 0.28e-9;
Ns = 4; delta_G0 = 3*kBT;
Lk = 0.7e-9; Ks = 150;

%%%%%%%%%%%%%%%%%%%%%%%%%%%%%%%%%%%%%%%%%%%%%%%%%%%%%%%%%%%%%%%%%%%%%%%%%%%%%%%
% B. Computation of native lengths
%%%%%%%%%%%%%%%%%%%%%%%%%%%%%%%%%%%%%%%%%%%%%%%%%%%%%%%%%%%%%%%%%%%%%%%%%%%%%%%
conf_ratio = exp(delta_G0/(kBT));
N_planar = Ns/(conf_ratio + 1); N_helical = Ns-N_planar;
Lp = 0.38e-9;
Lc = N_planar*L_planar + N_helical*L_helical; %contour length
r = sqrt(2*Lp^2*(exp(-Lc/Lp)-1+Lc/Lp)) %rms end to end length

%%%%%%%%%%%%%%%%%%%%%%%%%%%%%%%%%%%%%%%%%%%%%%%%%%%%%%%%%%%%%%%%%%%%%%%%%%%%%%%
% C. Force-Distance Curve and Force-Potential Curve for linker (PEG)
%%%%%%%%%%%%%%%%%%%%%%%%%%%%%%%%%%%%%%%%%%%%%%%%%%%%%%%%%%%%%%%%%%%%%%%%%%%%%%%

F = [0:1e-12:Funbind];

if linker == 0

    L_peg(1) = 0; U_peg(1) = 0;
    for n = 2:length(F)
    delta_G = delta_G0 - F(n)*(L_planar-L_helical);
    L_peg(n) = Ns*(L_planar/(exp(delta_G/kBT)+1) + L_helical/(exp(-
delta_G/...
           kBT)+1))*(coth(F(n)*Lk/kBT)-kBT/(F(n)*Lk))+Ns*(F(n)/Ks);
    U_peg_temp = cumtrapz(L_peg(1:n),F(1:n));
    U_peg(n) = U_peg_temp(end);
    end

else

    L_peg(1) = 0; U_peg(1) = 0;
```

```
    for n = 2:length(F)
    L_peg(n) = Lc*(coth(F(n)*Lk/kBT)-kBT/(F(n)*Lk))+Ns*(F(n)/Ks);
    U_peg_temp = cumtrapz(L_peg(1:n),F(1:n));
    U_peg(n) = U_peg_temp(end);

    end

end

%%%%%%%%%%%%%%%%%%%%%%%%%%%%%%%%%%%%%%%%%%%%%%%%%%%%%%%%%%%%%%%%%%%%%%%%%%%%%%%
% D. Force-Distance Curve and Force-Potential Curve for Bond
%%%%%%%%%%%%%%%%%%%%%%%%%%%%%%%%%%%%%%%%%%%%%%%%%%%%%%%%%%%%%%%%%%%%%%%%%%%%%%%

%We have no expression or solid data for this energy landscape. A simple
%linear model is used

    L_rc = 0.4e-9; k_bond = F(end)/L_rc;
    L_bond(1) = 0; U_bond(1) = 0;

    for n = 2:length(F)

    L_bond(n) = F(n)/k_bond;
    U_bond_temp = cumtrapz(L_bond(1:n),F(1:n));
    U_bond(n) = U_bond_temp(end);

    end

%%%%%%%%%%%%%%%%%%%%%%%%%%%%%%%%%%%%%%%%%%%%%%%%%%%%%%%%%%%%%%%%%%%%%%%%%%%%%%%
% D. Compute Force and Energy in Each PEG Molecule
%%%%%%%%%%%%%%%%%%%%%%%%%%%%%%%%%%%%%%%%%%%%%%%%%%%%%%%%%%%%%%%%%%%%%%%%%%%%%%%

L_total = L_peg + L_bond; U_total = U_peg + U_bond;
Lmax = L_total(end);

for n = 1:length(elongation)

    if elongation(n) <= Lmax

        F_out(n) = -interp1(L_total,F,elongation(n));
        U_out(n) = interp1(L_total,U_total,elongation(n));
        U_out_peg(n) = interp1(F,U_peg,-F_out(n));
        U_out_bond(n) = interp1(F,U_bond,-F_out(n));

    else %bond is broken

        F_out(n) = -1; U_out(n) = 0;
        U_out_peg(n) = 0; U_out_bond(n) = 0;

    end
end

F_out = F_out';

end
```

Appendix D

DNA origami additional information

D.1 Negative stain TEM images of DNA origami devices

Gel Purified and Diluted

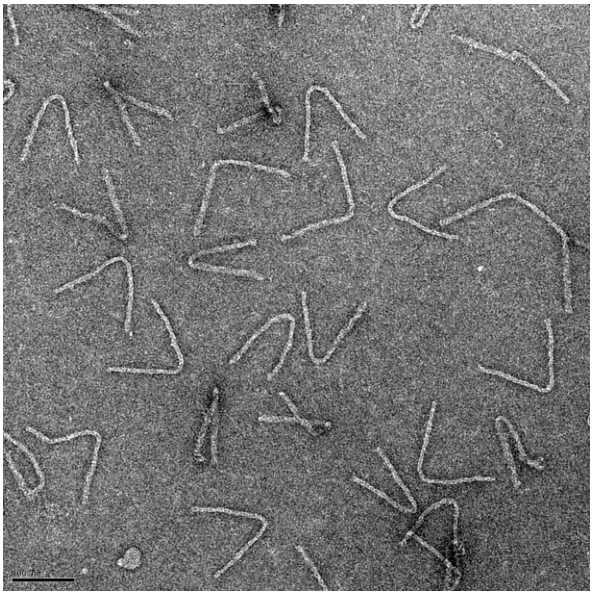

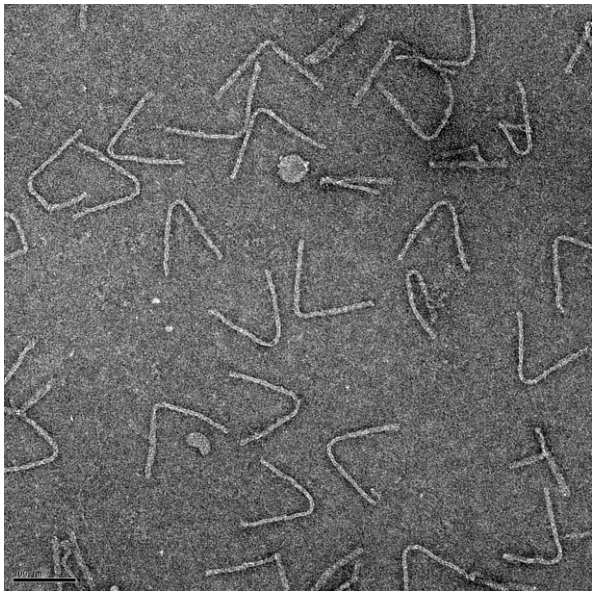

Not Diluted or Purified (post reaction)

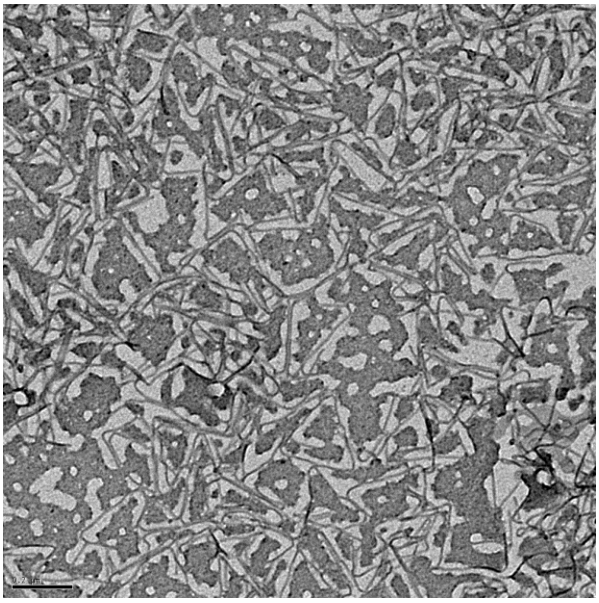

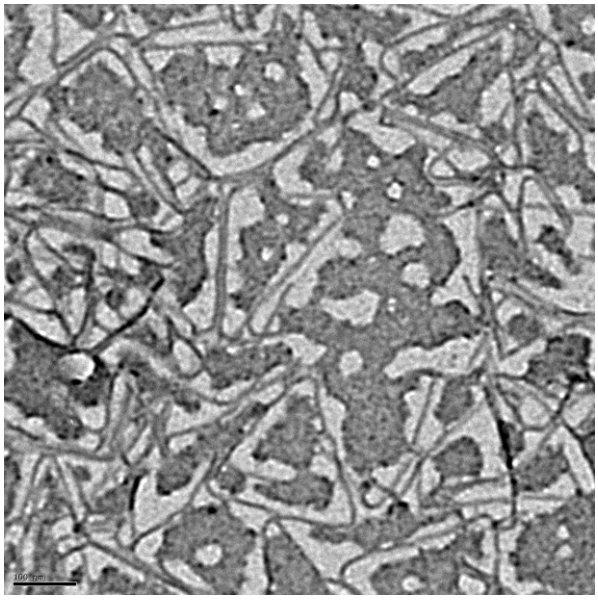

D.1: Primary layout for DNA origami device without toeholds.

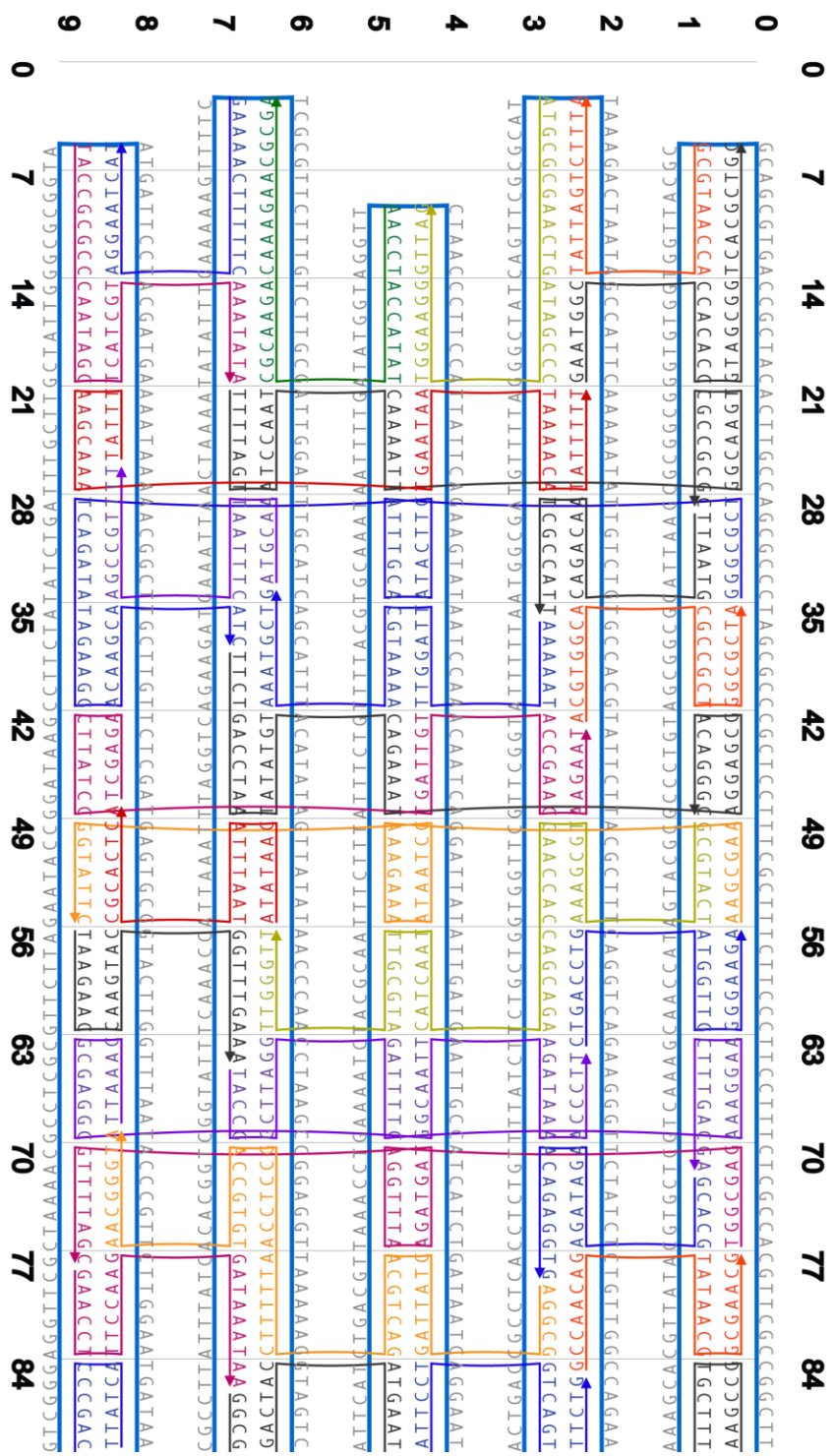

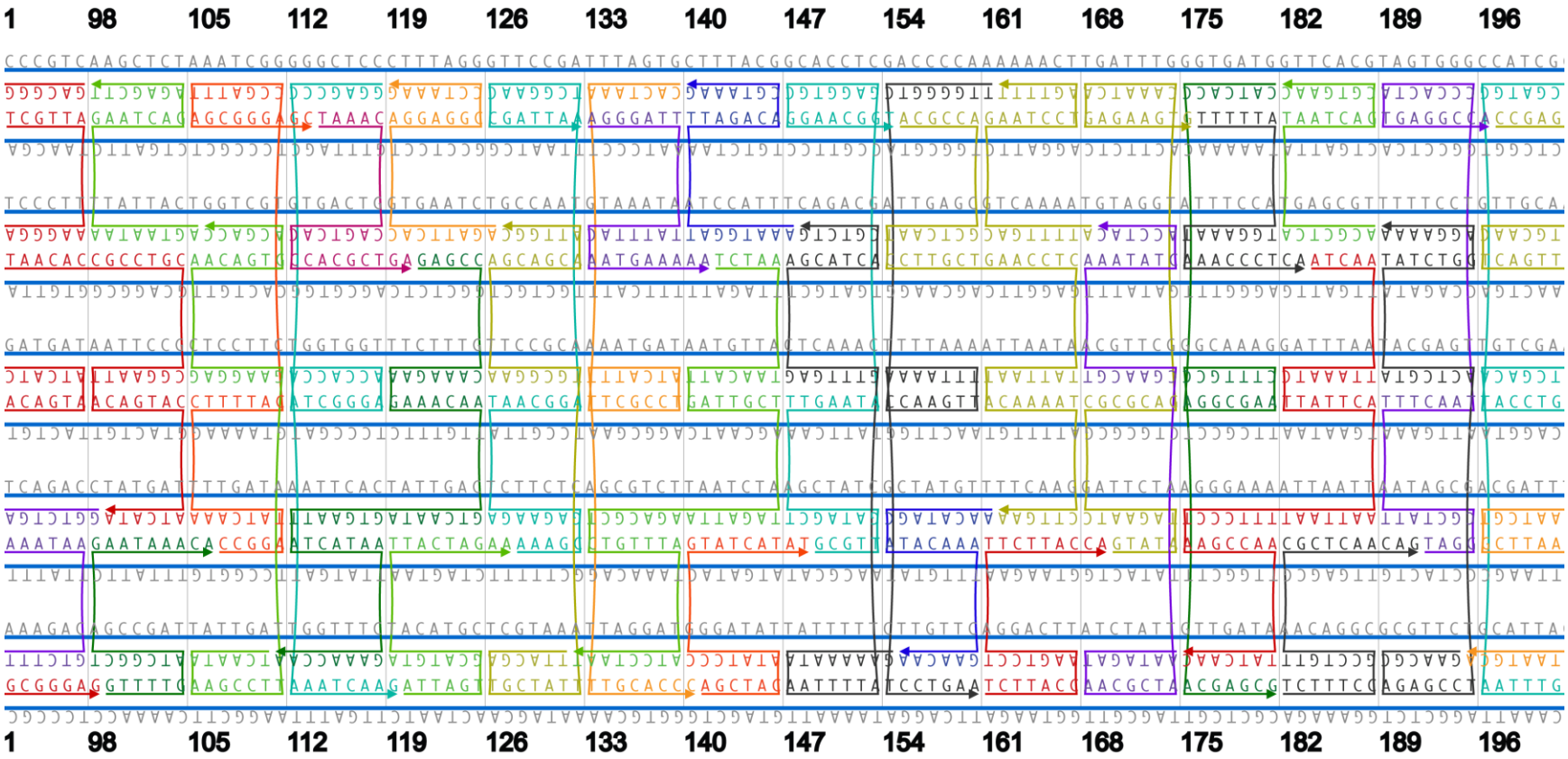
1
98
105
112
119
126
133
140
147
154
161
168
175
182
189
196

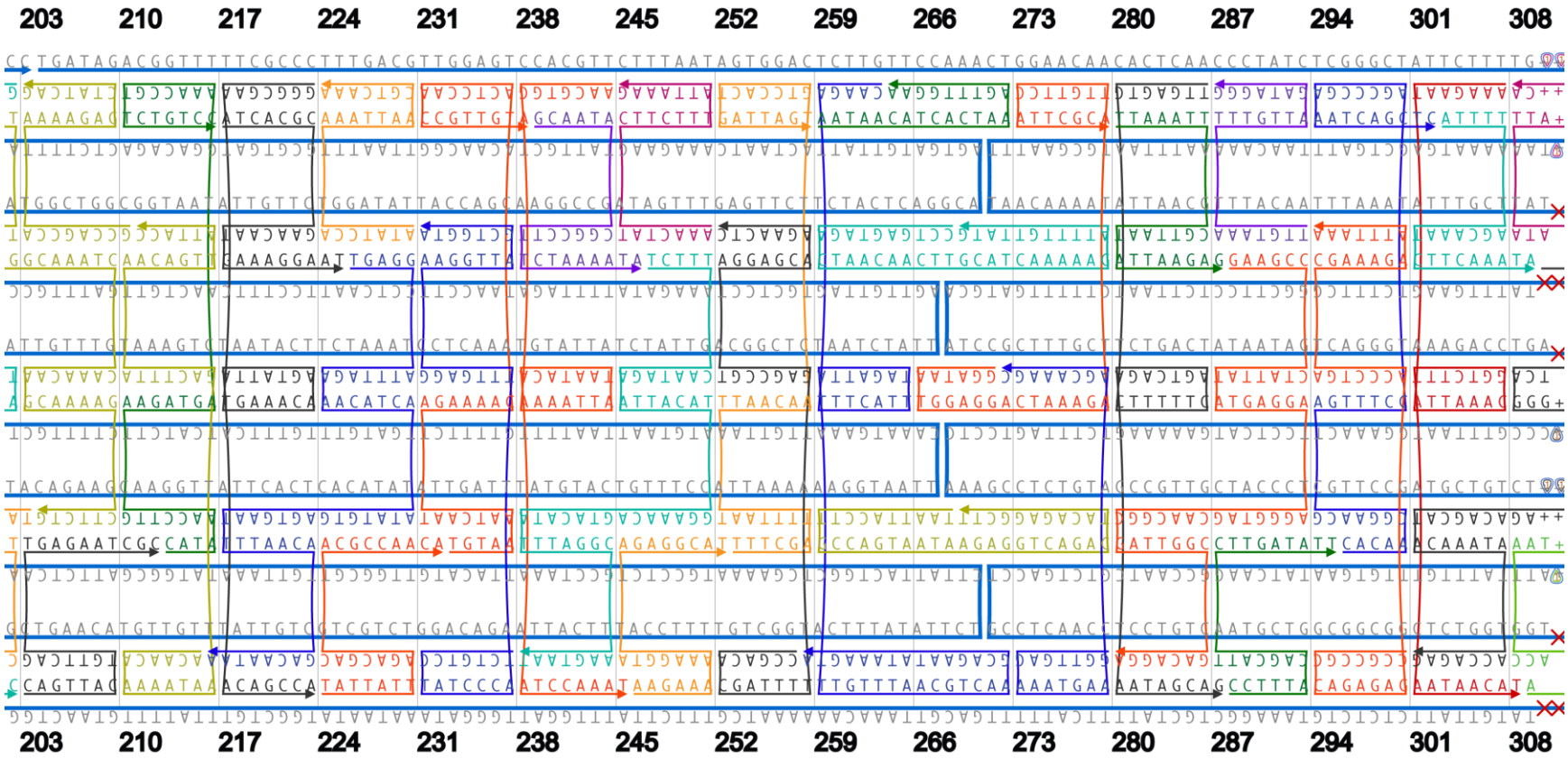
203
210
217
224
231
238
245
252
259
266
273
280
287
294
301
308

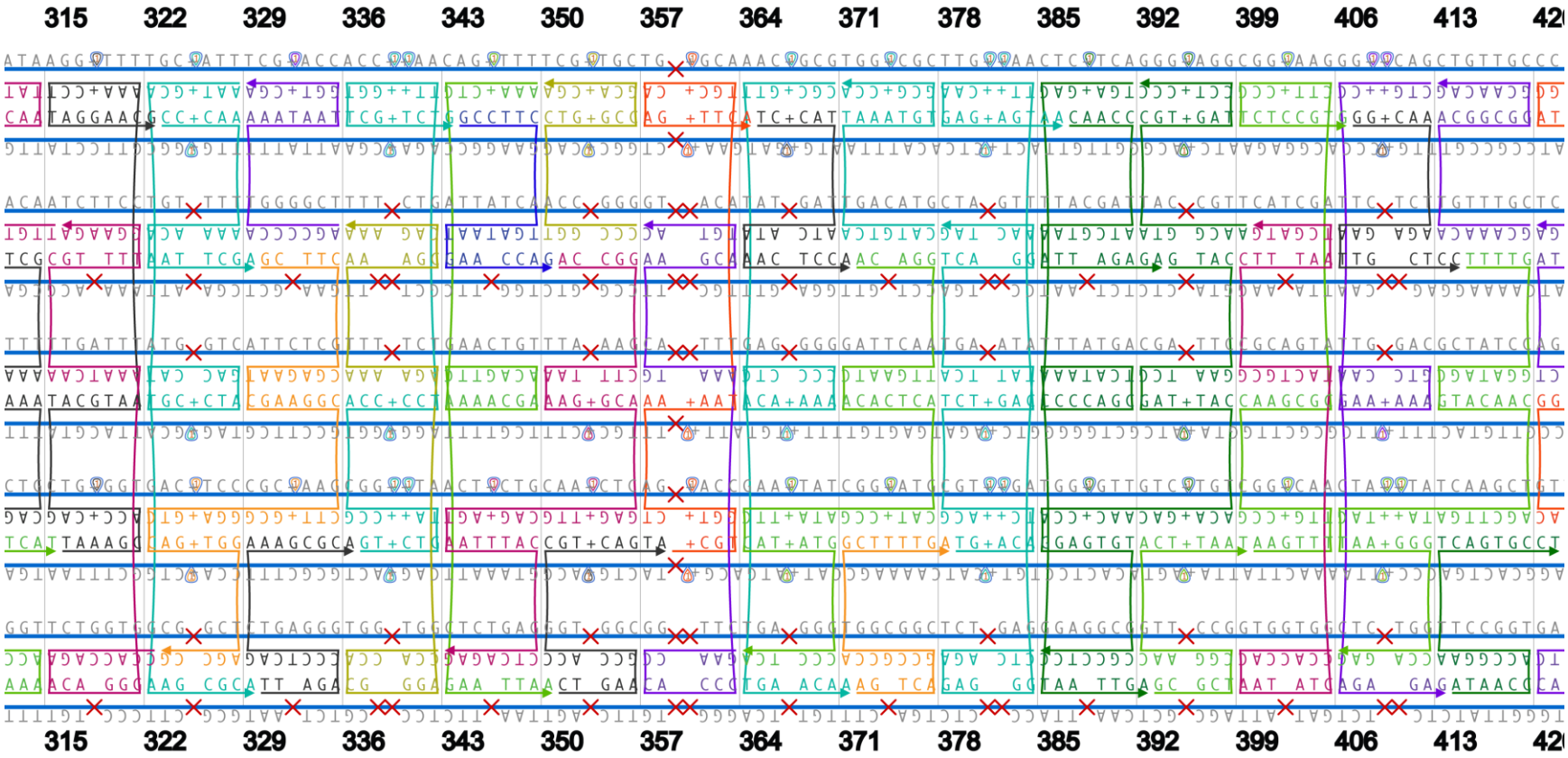
315
322
329
336
343
350
357
364
371
378
385
392
399
406
413
420

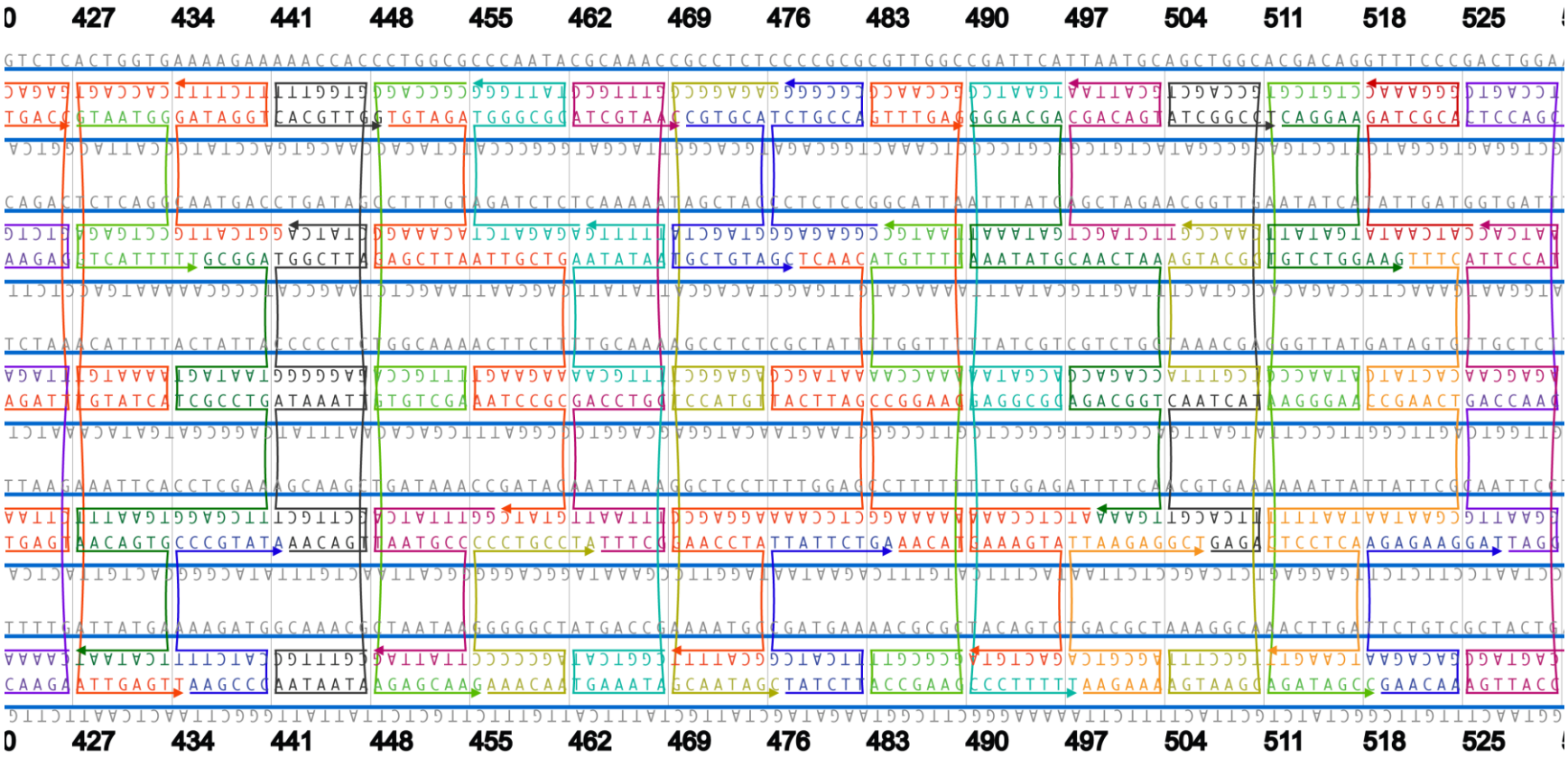
0
427
434
441
448
455
462
469
476
483
490
497
504
511
518
525

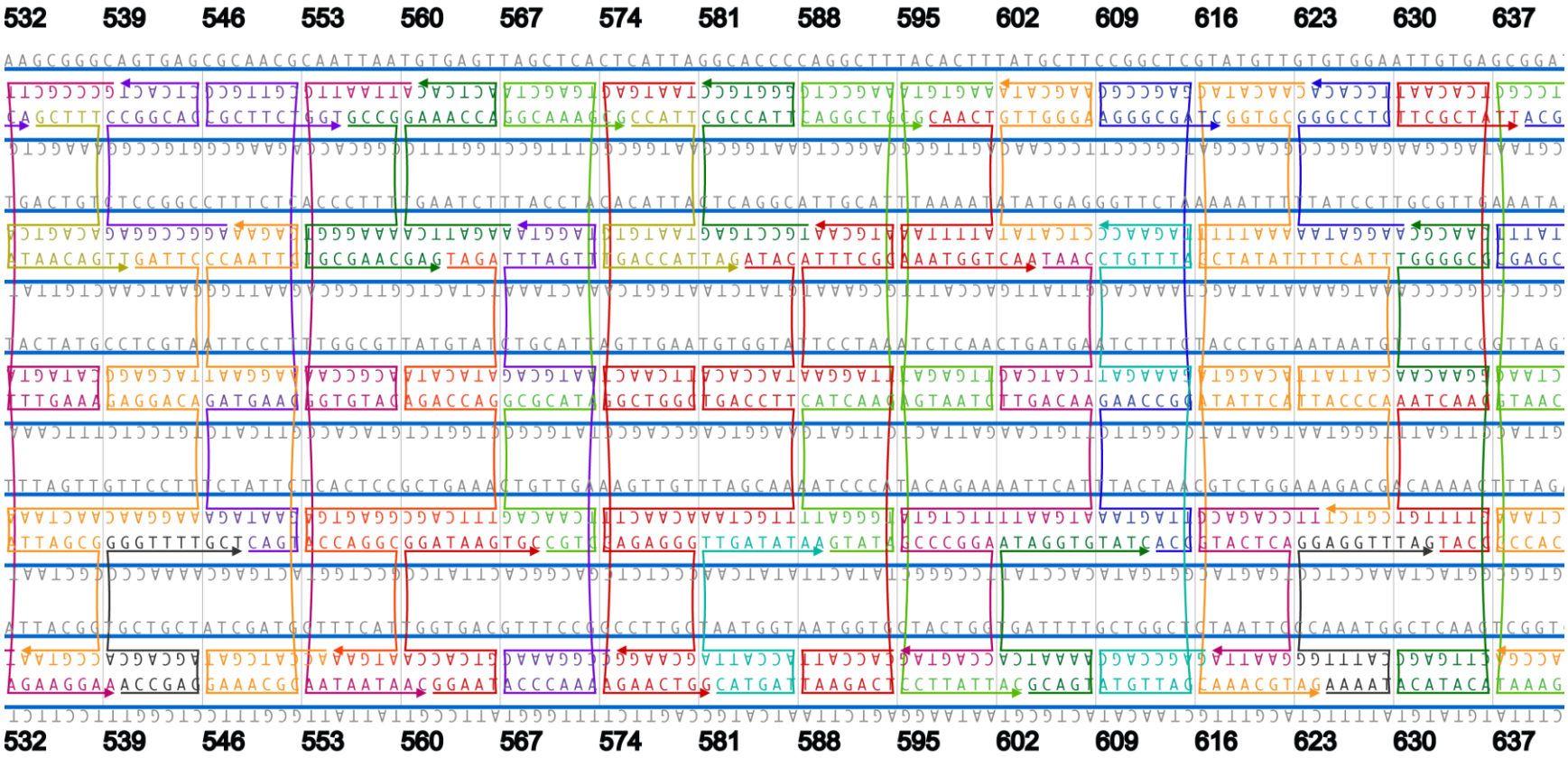
532
539
546
553
560
567
574
581
588
595
602
609
616
623
630
637

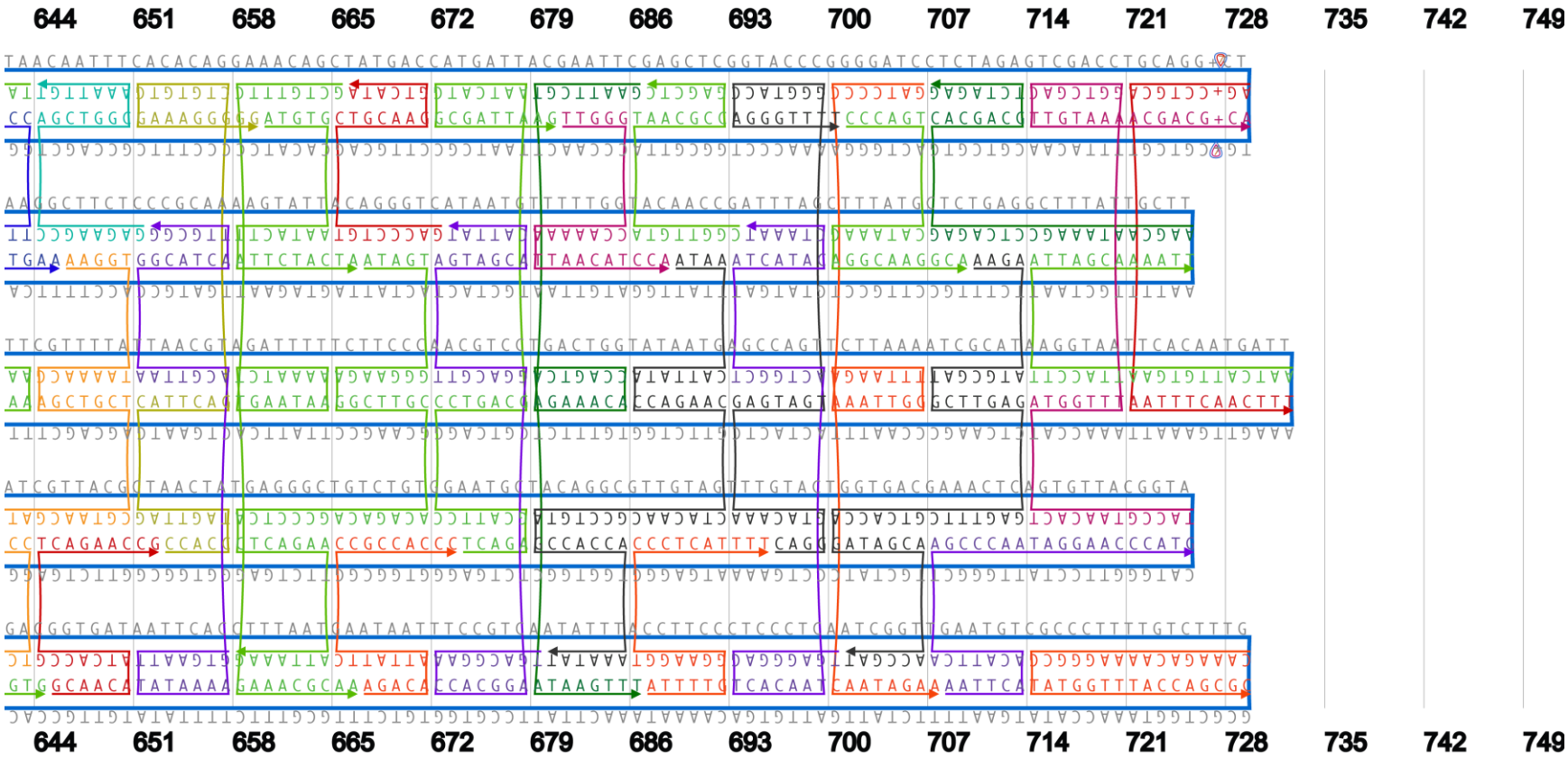
644
651
658
665
672
679
686
693
700
707
714
721
728
735
742
749

D.2: Strand sequence for device without oligonucleotides deletions for toehold formation

Oligo Name	Sequence (5'-3')
staple 1	GGGCGCTATTTGCAATACTTCTCAGATATAGAAGGACAAGCAATC
staple 2	AAGCGAAAAAGAAAATAATCCGGTATTC
staple 3	TGGCGAGAGGTTTAAGATGATGTTTTAGC
staple 4	GACGGGGTACAGTAATCATCATGCGGGAG
staple 5	GGAGCCCATCGGGAACCACCAAAATCAAG
staple 6	CACTAAATTCGCCTATCATTTTTGCACCC
staple 7	TTGGGGTCCCAAGTTTTTAAAATCCTGAA
staple 8	CATCACCAGGCGAACTTTGCCACGAGCG
staple 9	GCGATGGTACCTGATTCGACAAATTTGC
staple 10	GGGCGAATGAAACAAGTATTAACAGCCA
staple 11	AACGTGGAAAATTATAATACAATCCAAAT
staple 12	CAAGATTTCATTTAGATTATTGTTTAACGTCAAGCAGAATATAAAGTA
staple 13	TTGAGTGCTTTTTCAGTCAGAAATAGCAG
staple 14	AAAGAATATTAAACGGTCTTTAATAACAT
staple 15	AATCGGCATGCCACTAGACCATAAGCGCA
staple 16	AAATCCTGAAAACGAACAGTTCGAATTAA
staple 17	CGCTGGTTACACTAAACCCCTCTGAACAA
staple 18	TGAGAGAGCCCCAGCTCATAAATAATTGA
staple 19	CTGATTGCCGAAACAAAGTCCAAAGAGAG
staple 20	CACCAGTTGTATCAAAAATGTATTGAGTT
staple 21	CGCCAGGGTGTCGATTTGCCAAGAGCAAG
staple 22	GAGAGGCGTCCATGTAGAGGCTGCAATAGC
staple 23	TGAATCGGAGGCGCACGATAACCCTTTTT
staple 24	CTGTCGTAAGGGAAATAACCCAGATAGCC
staple 25	GCCCGCTTTTTGAAACATAGTAAGAAGGAA
staple 26	ATTAATTGGGTGTACACGCCAAAATAATAAC
staple 27	TAATGAGGGCTGGCTTCAACTAGAACTGG
staple 28	AAGTGTAAGTAATCTTGAGATCCTTATTAC
staple 29	CAACATACATATTCAACAGGTACAAACGTAG
staple 30	TATCCGCGTAACAAAACTAACTAAAGGTG
staple 31	GCTGTTTCTGAATAAAAAATCTGAAACGCAA
staple 32	GAATTCGTAGAAACACCAGTCAATAAGTTT
staple 33	GATCCCCAAATTGGTTTAAGACAATAGAA
staple 34	AGCTTGCATGCCTGCAAATTTCAACTTT
staple 35	GCGTAACCATATTAGTCTTTA
staple 36	TTAATGCAGACAATCGCCATT
staple 37	GCGTACTAAAGCGTGAACCACCAGCAGACATCAATTTGCGTATTGGGTT

staple 38	GCACGAGATAGAACAGAGGTG
staple 39	TCGTTAAAGGGACTTAACACCGCCTGCCGGAATTACAGTACATCATA
staple 40	TAAACCAGTCACCCACGCTGA
staple 41	AGGGATTTATTTACAATGAAAAA
staple 42	ACGCCAGCTCAATCCTTGCTGAACCTCTATTAATACAAAATCTTGAA
staple 43	TTTTTATGGAAATAAACCCTCA
staple 44	CCGAGTTTGCAACTCAGTTGGCAAATCCAAACAAGCAAAAGCTTCTG
staple 45	ATCACGCGAACAATGAAAGGAAT
staple 46	GCAATACGGCCTTTCTAAAATA
staple 47	AATAACATCACTAAAGTTTGGAA
staple 48	TTAAATTCGTTAATATTAAGAG
staple 49	ATTTTAGCAAATCTTCAAATA
staple 50	CCATCAAAAAACAAATTCGA
staple 51	GCCTTCTGATAATGAACCAG
staple 52	TCAACATATCATAAACTCCA
staple 53	CAACCATCGTAAATTAGAGA
staple 54	GGAACAAAGAGAATTGCTCC
staple 55	GTAATGGCCTGAGAGTCATTTTT
staple 56	TGTAGAACAAAGGGAGCTTAATTGCTGAAGAAGTAATCCGCGTATC
staple 57	CGTGCAGTAGCTATGCTGTAGC
staple 58	GGGACGAGATAAATAAATATGCAACTAACCAGACGAGACGGTTGAAA
staple 59	CAGGAATGATATTTGTCTGGAAG
staple 60	GCTTTACAGTCAATAACAGTT
staple 61	GCCGAAAGGGTTGCGAACGAG
staple 62	CCATTTAATGTGTGACCATTAG
staple 63	CAACTATTTTAAAAATGGTCAA
staple 64	GGTGCAAATTTTGCTATATTTTCATTCATTATTTTACCCACGTCT
staple 65	ACGCCTTTATTTCGAGCTGAA
staple 66	ATGTGAATACTTATTCTACTA
staple 67	TTGGGCCAAAAATTAACATCCA
staple 68	CCCAGTCATAAAGAGGCAAGGCA
staple 69	GAATGGCCCACACCGTAGCGGTCACGCTGC
staple 70	ACGTGGCACGCCGCTGGCGCTA
staple 71	CTGACCTGATGGTTGGGGAAGA
staple 72	GCCAACAGTATAACGGCGAACG
staple 73	AGTAATAAGAATCAGAGAGCTT
staple 74	AGATTCACAGGAGGCCCTAAAG
staple 75	AAATGGATTTAGACACGTAAAG
staple 76	ATTTTGACGAATCCTAGTTTT
staple 77	ACGCTCATAATCAGCGTGAAC
staple 78	GCCAGCCAAAAAGAGCTATCAG
staple 79	ATATCCAAAATTAACGTCAAA

staple 80	AAACTATCTTCTTTATTAAAG
staple 81	CCTGAGTAGACTAACAACTTGCATCAAAAAGATTTTGTTATG
staple 82	TTGTAAATTTGTTAGATAGGG
staple 83	TTGTATATTAACCAATATAAATCA
staple 84	AGCCCCAAAATAATGGTTCCGA
staple 85	CCCGGTCTGTAGCCGCAGGCGA
staple 86	CATGTCATAAATGTGCGGTCCA
staple 87	AACGGTACGTCGGATCCTGGCCC
staple 88	GCAAACAACGGCGGGCAACAG
staple 89	GGTCATTGGATAGGTTTCTTTT
staple 90	AGAGATCTTGGGCGCTATTGGG
staple 91	CGGAGAGGTCTGCCACGCGGG
staple 92	TTCTAGCTCGACAGTGCATTAA
staple 93	CATCAATAGATCGCAGGGAAAC
staple 94	AGGCCGGAGCCGGCACCTCACT
staple 95	AAGATTCAGAAACCAACTCAC
staple 96	TGCCTGAGCGCCATTGGGTGCC
staple 97	CTCATATGTTGGGAAAGCATA
staple 98	AAGGATAAGGGCCTCTCCACA
staple 99	GAGAAGCCAGCTGGCAAATTGT
staple 100	GACCCTGTCTGCAAGGTCATA
staple 101	CGGTTGTATAACGCCGAGCTC
staple 102	AAGCAATAAAGCCTCAGAGCACGACGTCTAGAG
staple 103	ATGCGCGAACTGATAGCCCTGGAAGGGTTAG
staple 104	AAAAATTTGGATTCGTAAAAAAATGCTG
staple 105	AGGCGGATTATCACGTCAGCTTTTTAACCTCCGACCGTGTAACGGGTA
staple 106	GAGCCCAAAGAAGAAACAAGTCAATAGTGAATTATCATAAGAAACCAA
staple 107	TCTAATAACATTGATTGCTTAGATTAAGACGCTCTGTTTAATCCTAAT
staple 108	ATCAATTAAATCTTATTCAAATTAATTTTCCCTAAGCCAATATCAAC
staple 109	TGAGGATTTAGAAACATCAATATGTGAGTGAATTTTAACAGACAATAA
staple 110	TCTTTCAATAGAATTACATGGAAACAGTACATATTTAGGCAAGTAAT
staple 111	GAAGCCCTATTATATGAGGAAGGGTAGCAACGGCGATTGGCGACAGGA
staple 112	TCGAAATCAGGGTAAAACAGCGAAAGACAGCATACAAATAACCAGAG
staple 113	GCTTCCGAGAATCGAAGGCCTTTTGCGGGATCGTCCAGAATGGAGCCG
staple 114	ACCGGCTTTAAAAGAGGCAGAGGCTTGCAGGGAGTAATTTACCTCAGAG
staple 115	ACAGGTTGAATCACACTCACATAACCGATATATTCCATACATGCCCTCA
staple 116	GTACGAATCGGATTATACACAATGACAACAACCAGGAGTGTCGCCTCC
staple 117	TTTTGGGATAGCGTACAACAGCTTGATACCGATAGTAACGGGGCCAGAG
staple 118	GCGGATAATAGTTCGCCTGTTCGAGGTGAATTTAACAGTGTCATAAT
staple 119	TCAACAATAGCGTACTTAGCTCCAAAAGGAGCCGAACCTAGCATTTT
staple 120	TTTCCACTATCCCGAACTCGAATAATAATTTTCTCCTCATCAAGTT
staple 121	GATTCTACGAGGGAGGACAAAGGAACAACTAAAATTAGCGCCGTAA

staple 122	TAGAATACATAAGACCAGTTTCAGCGGAGTGAACCAGGCATGAA
staple 123	ATACTACCACATGACCTTTTGCTAAACAACTTGAGAGGGGCAAGG
staple 124	TAACTCATCAGTTGACAAATGAATTTTCTGTAGCCCGGACCAGTAG
staple 125	AAGGTTAAAACGAGCTGCTCGTAACGATCTAAAGCCACCCTCACCGA
staple 126	ATAGTGGGAAGAGGCTTGCACAGACAGCCCTCACTCAGAAATTAAAG
staple 127	ATAACATTATACCAGAACCTACAACGCCTGTAGCCACCAAAATAT
staple 128	AAGAATGCGATGCTTGAGGAGTTTCGTCACCAGATAGCAACCGAT
staple 129	GGATAATGGAGGACTAAAGATTGTTCCATTCGCA
staple 130	AATCATTGTGAATTACCTTATTAGCAAAATT
staple 131	AACCTACCATATCGCAAGACAAAGAACGCGA
staple 132	ATGCAATAATTTCAGCCGTTTT
staple 133	ATATAACATTTAATCGCACTCA
staple 134	GGTCTGAGTAAATAAGTCTTTCC
staple 135	AACATAGCATACAAAGAACAA
staple 136	TAAATCGTGCTTAATCTAATGCA
staple 137	TAATTACCTTGCCAGTAATAAGAGGTCAGACTACAGAGGCTT
staple 138	GGTTTATCATAATGCCTTATTAG
staple 139	ATCTCCAAAGAAAGTAGACTGTA
staple 140	TTCCAGACGGTACTCAGAATTA
staple 141	TACCGTAACACTATGGTTTGGTCGACTTGTAAAACGACGGCCAGTGCCA
staple 142	GAAAACTTTTTCAGGAATCAT
staple 143	TTTTAGTATCCAATCAAAATTGGCAAGTCGCCGCGC
staple 144	TTCTGACCTAATATATGTCAGAAATAGGAGCGACAGGGC
staple 145	TACCGGCTTAGGGATTTTCAAAGGAACTTTGACGA
staple 146	GGCGTAGACTACATGAATAAAAGCCGTGCTTTCC
staple 147	CCGGATATCAAACTTTTACCCGATTTAGCGGGAGC
staple 148	AAAGCGAGAAGATAACGGATCGGAACCGATTAA
staple 149	GCGTTGATAGCTTTGAATAGAGGTGCGGAACGGT
staple 150	GTATATAGAATCCGCGCAGCAAATCAGAGAAGTG
staple 151	TAGGCGCTATTTTTCAATCCCACTATGAGGCCA
staple 152	CATAAACCTTGAAGATGAAAACCGTTCTGTCC
staple 153	TGTAAAATCAATAGAAAACACTCCAACCGTTGTA
staple 154	TTTCGATTTTAATTTAACAAGTCCACTGATTAGT
staple 155	CACAACGGAACGAGTTTCCAGCCCGAAATCAGCTC
staple 156	TAAAGCACCCTCAGTACGTAAAAATCCCTTAGGAACG
staple 157	GTCTCTGTAAAGGCCGACCAACCTTTTGATGGTTCGCGTCTG
staple 158	AGCGTGGTCGCTAAAGAATTGCCCCAAGCTTTCA
staple 159	TGATACATCGCCCACGTCTTTGACTTGCAGCAAGAGCGAGTAA
staple 160	AAGTTTTTGCGCCGCAAGCGCCTTCACCGTCTCCGTG
staple 161	TGAGTCTTAAACGGAGATTGAGACGGATTGACC
staple 162	AACAGTGCTTGCTATAAATTGTGGTTTCACGTTGG
staple 163	TTTCGTTTAATTGACCTGCGTTTGCGATCGTAAC

staple 164	AACATAAAAAGGCCGGAACGCCAACGGTTTGAG
staple 165	GAGATTCACGTCAATCATGCCAGCTATCGGCCT
staple 166	TAGGGGAATTGGACCAACTCCAGTCCTCCAGCCA
staple 167	CAGTGAATAGAGATGAACCGTTGCGCGCTTCTGGT
staple 168	CGTCTCAACAGGCGCATATGAGCTAGGCAAAGCG
staple 169	GTATATGGGATTCATCAAGAAGCCTGCAGGCTGCG
staple 170	ACCTTAGTAAGAACCGGGAGCCGGAGGGCGATC
staple 171	TACCGTTTTGTAATCAACTCACAATTTCGCTATT
staple 172	CCACCTAGTTAGCATTCAGCTGTGTGGAAAGGGGG
staple 173	TCAGAGCATTCCCCTGACGAATCATGGCGATTAAG
staple 174	CAGGGTACAAAGAGTAGTGGGTACCAGGGTTTT
staple 175	TATTTAAGCAAATGAATAATAAAACATATTTTT
staple 176	TCGAGACTTATCCTGATTGTACCGAACAAGAAT
staple 177	TTAAACGCGAGGCGGCAATTAGATAAAACCCTT
staple 178	TTATCACCCGACTTATTCCTGTCAGTAATTCTG
staple 179	TCAATAAAGCCTTGAAGGAGAACAGTGACGACC
staple 180	TTACGATGCTATTTGCGGAAAGCAGCAATTGGC
staple 181	GAAAAATAAATTTTAGTTTGAGAGCATCACGTCTG
staple 182	AATAGATAACGCTACGAACGTAAATATCACCTAC
staple 183	GAACGCAGAGCCTACTCGTATATCTGGAGGAAAA
staple 184	ACAACAAAAATAAGACTTTAAACAGTTATTACC
staple 185	TCTGTCCTATCCCATTTGAGGAAGGTTAGCTGGTA
staple 186	CCGACACGATTTTGAGCCGTAGGAGCAAGAACTC
staple 187	GGTTGAGAAATGAAAGCAAAGC
staple 188	CCGCCGCCAGAGAGACCCTGACGAAAGAATTTAAA
staple 189	CCACCAGAACAGGGAAATCAACGTTTTGGAAGA
staple 190	CCACCACGGGAAGAAAAAAAGCCAGAAA
staple 191	GAACCCACCCAAATGAAGCATGTAC
staple 192	CTCAGAGAGGGTATTCATCAGGAACTAG
staple 193	CCACCACAATATCTACTGCGCTTTAATCGATG
staple 194	CAAAATCCACAAGATTAGACTATAAGAGGTCTGGA
staple 195	CGTTTGCAATAATAGAGGGGGTGGCTTACTATCA
staple 196	CGGTCATTGAAATATTTGCAAAATATAATTTTTG
staple 197	GCGCGTTACCGAAGAAACCAAATGTTTTTAATGC
staple 198	TGCCTTTAGTAAGCTCGTTTAAGTACGGCAACCG
staple 199	TCAGTAGCAGTTACCAGAGCAAATTCCATAATCAC
staple 200	ACCATCGATGAAACGCAAGGAATCCAATTCGAGAA
staple 201	CCGGAAACACCCAAAAATGCAGTTTAGTTTAGGTA
staple 202	CACCATTTAAGACTTTAGGAAATTTCGCATGCAA
staple 203	GAGCCAGCATGTTAGGAAAGATCTGTTTATAGAACC
staple 204	CTTGAGCACATACAGGAACAATGGGGCGCAACGC
staple 205	GTGAATTTATAAAAACGTTAAGGCATCATTGCGG

staple 206	TGACGGAACCACGGAGGACGTTAGTAGCACATTAT
staple 207	TGAGGGAGTCACAATACTGGCTATCATACCTAAAT
staple 208	CAAAGACAAAAGGGCGTATGGTTTACCAGCGC
staple 209	TACCGCGCCCAATAGCTCATCGTAAATATA
staple 210	TAAGAACCAAGTACGGTTTGAAA
staple 211	GAACCTTTCCAAGGATAAATAA
staple 212	GTTTTGATCGGCTGAATAAACA
staple 213	ATTAGTGCATGTATTACTAGAA
staple 214	AGCTACATATCCCGTATCATAT
staple 215	TCTTACCAAGTCCTTTCTTACCA
staple 216	TCTTTCCGCCTGTTCGCTCAACAG
staple 217	CAGTTACTGTTCAGTGAGAATCGC
staple 218	TATTATTAGACGACACGCCAACA
staple 219	AAGAAAAAAGGTAAGAGGCAT
staple 220	CCTTTACAGCATTCTTGATATT
staple 221	AAAAACCACCAATCCTCAT
staple 222	TTAGACCCTCAGAAAGCGCA
staple 223	CTGAAGCCACCCGTTCCAGTA
staple 224	AGTCAGCCGCCAGCTTTTGA
staple 225	GCGCTCGGAACACTGGTAAT
staple 226	ATAACCACCGGAATCAGTGCCT
staple 227	AAGCCCCATCTTTCCCGTATA
staple 228	AAACAAAGCCCCCCCCTGCCTA
staple 229	TATCTTTTCATCGTTATTCTGA
staple 230	AAGAAAAGCGTCATTAAGAGGCT
staple 231	GAACAAGACAGAAAGAGAAGGAT
staple 232	ACCGAGAGCAGCAGGGTTTTGCT
staple 233	GGAATGTCACCAGGATAAGTGC
staple 234	CATGATACCATTATTGATATAA
staple 235	GCAGTAAAATCAATAGGTGTATC
staple 236	AAAATCATTTGGGGAGGTTTAG
staple 237	GCAACAATCACCGTCAGAACCG
staple 238	AGACAATTATTCCCGCCACCC
staple 239	ATTTTGGGAAGGTCCCTCATTTT
staple 240	AATTCAACATTCAAGCCCAATAGGAACCCATG

D.3: Oligonucleotide deletions and insertions for device design with 7nm toehold spacings

Removed Primary Strands:

staple 37	staple 121	staple 125	staple 105
staple 39	staple 109	staple 126	staple 106
staple 64	staple 122	staple 127	staple 119
staple 42	staple 110	staple 103	staple 107
staple 56	staple 123	staple 128	staple 120
staple 44	staple 124	staple 104	staple 108
staple 58			

Added Strands:

th15_1	TGTAGAACAAAGCGAGCTTAA
th15_2	TTGCTGAAAATACATGGCAGAAGAGGAAAAGCCAAGGAGTACCCCAATGTGA
th15_3	TCTTCTGCCATGTATTGAAGAAGTAATCCGCGTATC
th15_4	TCAACAATTGAGGTGTCCTAAACGGAAAAGCCAAGGAGTACCCCAATGTGA
th15_5	GTTTAGGACACCTCAATAGCGTACTTAGCTCCAAAAGGAGCCGAACCTAGCATTTT
th15_6	GGGACGAGATAAATAAATATG
th15_7	CAACTAACCTTACGCGGCCATAACAGGAAAAGCCAAGGAGTACCCCAATGTGA
th15_8	TGTTATGGCCGCGTAAAGACGAGACGGTTGAAA
th15_9	CCACCTTAGCCGTCTCGGGGGAAAAGCCAAGGAGTACCCCAATGTGA
th15_10	CCCGAGACGGCTAAGGCTATCCCGAACTCGAATAATAATTTTCTCCTCATCAAGTT
th15_11	GATTCTAGGAATAAGTGACCTATGGAAAAGCCAAGGAGTACCCCAATGTGA
th15_12	ATAGGTCACTTATTCCCGAGGGAGGACAAAGGAACAACTAAAATTAGCGCCGTAA
th15_13	TAGAATGCACCAGACGCCGCTTGGAAAAGCCAAGGAGTACCCCAATGTGA
th15_14	AAGCGGCGTCTGGTGCACATAAGACCAGTTTCAGCGGAGTGAACCAGGCATGAA
th15_15	ATACTAGCGATTTCGACCAACAGGAAAAGCCAAGGAGTACCCCAATGTGA
th15_16	TGTTGGTCGAAATCGCCCACATGACCTTTTGCTAAACAACTTGAGAGGGGCAAGG
th15_17	TAACTCGCGGGAACGGCTGTGCGGAAAAGCCAAGGAGTACCCCAATGTGA
th15_18	GCACAGCCGTTCCCGCATCAGTTGACAAATGAATTTTCTGTAGCCCGGACCAGTAG
th15_19	GGTGCAAATTTTGCTATATTT
th15_20	TCATTCAAGTCACACCGCTGTGTGGAAAAGCCAAGGAGTACCCCAATGTGA
th15_21	ACACAGCGGTGTGACTTTATTTTACCCACGTCT
th15_22	AAGGTTAAGCGGACAGTCTGAGCGGAAAAGCCAAGGAGTACCCCAATGTGA
th15_23	GCTCAGACTGTCCGCTAAACGAGCTGCTCGTAACGATCTAAAGCCACCCTCACCGA
th15_24	ATAGTGGTACCCTCTCAAGCACGGGAAAAGCCAAGGAGTACCCCAATGTGA
th15_25	CGTGCTTGAGAGGGTAGAAGAGGCTTGCACAGACAGCCCTCACTCAGAAATTAAAG
th15_26	ATAACAAGATCTACAGGGCGGGGGAAAAGCCAAGGAGTACCCCAATGTGA
th15_27	CCCGCCCTGTAGATCTTTATACCAGAACCTACAACGCCTGTAGCCACCAAAATAT
th15_28	AAGAATGTAGAAGCCGTCGCTTGGAAAAGCCAAGGAGTACCCCAATGTGA

th15_29	AAGCGACGGCTTCTACGCGATGCTTGAGGAGTTTCGTCACCAGATAGCAACCGAT
th15_30	TCTTTCACGGGTCCATGCGGGGGGGAAAAGCCAAGGAGTACCCCAATGTGA
th15_31	CCCCCGCATGGACCCGATAGAATTACATGGAAACAGTACATATTTAGGCAAGTAAT
th15_32	TGAGGATGTAAAACCCTGTTTAAGGAAAAGCCAAGGAGTACCCCAATGTGA
th15_33	TTAAACAGGGTTTTACTTAGAAACATCAATATGTGAGTGAATTTTAACAGACAATAA
th15_34	CCGAGTTTGCAACTCAGTTGG
th15_35	CAAATCCAGAGGTCCGGGCAGCATGGAAAAGCCAAGGAGTACCCCAATGTGA
th15_36	ATGCTGCCCGGACCTCAACAAGCAAAAGCTTCTG
th15_37	ATCAATTACGCGCGGCACCCATCGGAAAAGCCAAGGAGTACCCCAATGTGA
th15_38	GATGGGTGCCGCGCGTAAATCTTATTCAAATTAATTTTCCCTAAGCCAATATCAAC
th15_39	ACGCCAGCTCAATCCTTGCTG
th15_40	AACCTCTATCTCTTCATTCGCTTAGGAAAAGCCAAGGAGTACCCCAATGTGA
th15_41	TAAGCGAATGAAGAGATTAATACAAAATCTTGAA
th15_42	TCTAATATTGTGAACGTTCGAAAGGAAAAGCCAAGGAGTACCCCAATGTGA
th15_43	TTTCGAACGTTCACAAACATTGATTGCTTAGATTAAGACGCTCTGTTTAATCCTAAT
th15_44	GAGCCCAGCACAATGTGGTTTATGGAAAAGCCAAGGAGTACCCCAATGTGA
th15_45	ATAAACCACATTGTGCAAGAAGAAACAAGTCAATAGTGAATTATCATAAGAAACCAA
th15_46	TCGTTAAAGGGACTTAACACC
th15_47	GCCTGCCGGTGCTACTGTGGAGAGGGAAAAGCCAAGGAGTACCCCAATGTGA
th15_48	CTCTCCACAGTAGCACGAATTACAGTACATCATA
th15_49	AGGCGGAGGTTTGTGAATCTAGGGGAAAAGCCAAGGAGTACCCCAATGTGA
th15_50	CCTAGATTCACAAACCTTATCACGTCAGCTTTTTAACCTCCGACCGTGTAACGGGTA
th15_51	GCGTACTAAAGCGTGAACCAC
th15_52	CAGCAGACAAGCACAAAAAAGCGGCGGAAAAGCCAAGGAGTACCCCAATGTGA
th15_53	GCCGCTTTTTTGTGCTTCAATTTGCGTATTGGGTT
th15_54	AAAAATTTGCACTTCAGGCATAAAGGAAAAGCCAAGGAGTACCCCAATGTGA
th15_55	TTTATGCCTGAAGTGCGGATTCGTAAAAAAATGCTG
th15_56	ATGCGCGAACTGATAGCCCTGAGGATGGA
th15_57	TTTTTGACGGAAAAGCCAAGGAGTACCCCAATGTGA
th15_58	GTCAAAAATCCATCCTGAAGGGTTAG